Werk

Jahr: 1984
Kollektion: fid.geo
Signatur: 8 Z NAT 2148:54
Digitalisiert: Niedersächsische Staats- und Universitätsbibliothek Göttingen
Werk Id: PPN1015067948_0054
PURL: http://resolver.sub.uni-goettingen.de/purl?PPN1015067948_0054

LOG Id: LOG_0031
LOG Titel: Three-dimensional analysis of magnetometer array data
LOG Typ: article

Übergeordnetes Werk

Werk Id: PPN1015067948
PURL: http://resolver.sub.uni-goettingen.de/purl?PPN1015067948
OPAC: http://opac.sub.uni-goettingen.de/DB=1/PPN?PPN=1015067948

Contact

Niedersächsische Staats- und Universitätsbibliothek Göttingen
Georg-August-Universität Göttingen
Platz der Göttinger Sieben 1
37073 Göttingen
Germany
Email: gdz@sub.uni-goettingen.de

J Geophys (1983) 54: 138–156

Journal of Geophysics

Three-dimensional analysis of magnetometer array data

A.D. Richmond[1] **and W. Baumjohann**[2]*

[1] NOAA Space Environment Laboratory, 325 Broadway, Boulder, CO 80303, USA
[2] Institut für Geophysik der Universität Münster, Corrensstr. 24, D-4400 Münster, FRG

Abstract. A technique is developed for mapping magnetic variation fields in three dimensions using data from an array of magnetometers, based on the theory of optimal linear estimation. The technique is applied to data from the Scandinavian Magnetometer Array. Estimates of the spatial power spectra for the internal and external magnetic variations are derived, which in turn provide estimates of the spatial autocorrelation functions of the three magnetic variation components. Statistical errors involved in mapping the external and internal fields are quantified and displayed over the mapping region. These errors are particularly significant for the internal component, an inevitable consequence of the limited station coverage and of the smallness of the internal component with respect to the external component. Examples of field mapping and of separation into external and internal components are presented. A comparison between the three-dimensional field separation and a two-dimensional separation from a single chain of stations shows that significant differences can arise in the inferred internal component, although for the present data set these differences are generally less than the statistical mapping errors. The technique is compared with other methods of analysis, and possible future improvements are pointed out, particularly concerning allowances for local anomalies and for frequency dependence of the spatial power spectra.

Key words: Magnetometer arrays – Inverse theory – Magnetic field mapping – External and internal magnetic field separation – Optimal linear estimation – Spatial power spectrum – Spatial correlation

Introduction

Spatial patterns of magnetic variations, when properly analyzed, can provide considerable information about electric current systems in the ionosphere and magnetosphere, as well as about the conductivity structure within the earth. The main observational source of information about these patterns comes from arrays of magnetometers spread over some portion of the earth's surface, providing point measurements of the magnetic field continuously in time. To infer the spatially continuous patterns from these point measurements and to determine the accuracy of the inferred patterns is a significant problem in geophysics. The primary purpose of this paper is to develop a practical approach to this problem and to demonstrate its application to a data set from the Scandinavian Magnetometer Array (Küppers et al., 1979). The technique we develop tends to minimize the inevitable error of estimating continuous functions from point measurements by incorporating previously determined geophysical information in the process, and by using statistical information obtained from the data at hand. Being able to quantify the horizontal spatial characteristics of the magnetic perturbations allows us to proceed with further types of analysis which would not otherwise be possible. The field can be separated into an "external" part, associated solely with overhead currents, and an "internal" part, associated solely with currents induced within the earth, below the plane of observation. The external component can be continued up to the base of the overhead current region in the ionosphere by using the potential field approximation (e.g. McNish, 1938; Nagata, 1950). This upward continuation can bring more sharply into focus concentrated ionospheric currents like electrojets (e.g. Mersmann et al., 1979) and even reveal small-scale features within the electrojet (e.g. Sulzbacher et al., 1980) which may be overlooked in the ground-level field. For earth conductivity studies quantitative knowledge of the wave number spectrum of magnetic variation fields is often important (e.g. Wait, 1962; Price, 1962, 1967; Srivastava, 1965; Rikitake, 1966; Hermance and Peltier, 1970; Hutton, 1972; Schmucker, 1973; Hibbs and Jones, 1978; Beamish, 1979; Quon et al., 1979; Lange, 1979; Rokityansky, 1982) but this knowledge has in the past been inaccessible or difficult to obtain. The technique we develop allows an estimation of this spectrum.

In previous studies which analyzed magnetic variations from several stations simultaneously to determine the external and internal components, the basic approach involved either fitting model currents with adjustable parameters to the data, or else performing an unrestricted mathematical analysis with some sort of smooth interpolation between stations. Model fitting of two or three-dimensional currents has been performed,

* *Present address:* Max-Planck-Institut für Physik und Astrophysik, Institut für extraterrestrische Physik, 8046 Garching, Federal Republic of Germany

Offprint requests to: A.D. Richmond

Table 1. List of Scandinavian Magnetometer Array stations used in this study

Station Name	Symbol	Lat.	Long.	x (km)	y (km)	*	A	B	Z
Malöy	MAL	62.18	5.10	−350	−887	C	×	×	×
Hellvik	HEL	58.52	5.77	−735	−1,033	C	×	×	×
Namsos	NAM	64.45	11.13	−239	−509	C	×	×	×
Arvika	ARV	59.60	12.60	−774	−623		×	×	×
Okstindan	OKS	65.90	14.27	−136	−317		×	×	×
Risede	RIS	64.50	15.13	−296	−326		×	×	×
Hassela	HAS	62.07	16.50	−575	−338		×	×	×
Lovö	LO	59.35	17.83	−888	−348		×	×	×
Andenes	AND	69.30	16.02	202	−134	C			×
Evenes	EVE	63.53	16.77	112	−129		×	×	×
Ritsemjokk	RIT	67.70	17.50	15	−124		×	×	×
Storavann	STO	65.78	18.18	−198	−150		×	×	×
Lycksele	LYC	64.57	18.68	−335	−160		×	×	×
Mikkelvik	MIK	70.07	19.03	255	0	C	×	×	×
Rostadalen	ROS	68.97	19.67	130	− 4		×	×	×
Nattavaara	NAT	66.75	21.00	−122	− 3		×	×	×
Pitea	PIT	65.25	21.58	−291	− 10		×	×	×
Nurmijärvi	NU	60.50	24.65	−839	51		×	×	×
Bear Island	B4	74.52	19.02	736	116	C	×	×	×
Söröya	SOR	70.60	22.22	287	129	C	×	×	×
Mattisdalen	MAT	69.85	22.92	200	139		×	×	×
Mieron	MIE	69.12	23.27	118	139		×	×	
Muonio	MUO	68.03	23.57	− 2	131		×	×	×
Pello	PEL	68.85	24.73	−140	159		×	×	
Oulu	OUL	65.10	25.48	−337	166		×	×	×
Sauvamäki	SAU	62.30	26.65	−654	184		×	×	×
Skarsvag	SKA	71.12	25.83	324	268	C	×	×	×
Kunes	KUN	70.35	26.52	236	282		×	×	
Kevo	KEV	69.75	27.03	167	294		×	×	×
Sondankylä	SO	67.37	26.63	− 93	248		×	×	×
Vadsö	VAD	70.10	29.65	197	397		×	×	×
Loparskaya	LOP	68.60	33.30	25	534		×	×	×
Lovozero	LZ	67.98	35.02	− 42	606		×	×	×

* Coastal stations noted with "C" are assigned extra truncation error in the Z component (see text)
"A" (northward), "B" (eastward), and "Z" (downward) data are available if so noted with "×"

for example, by Walker (1964), Czechowsky (1971), Horning et al. (1974), Fambitakoye and Mayaud (1976), Oldenburg (1976a), Bannister and Gough (1977, 1978), Gough and Bannister (1978), Loginov et al. (1978), Maurer and Theile (1978), Hughes et al. (1979), Akasofu et al. (1980), and Baumjohann et al. (1981). A disadvantage of the model-fitting approach up to now has been the necessity to restrict greatly the number of parameters allowed in the model, in particular making very simple assumptions about earth currents. Unrestricted mathematical analyses of external and internal variations so far have been performed primarily either in two dimensions over a relatively limited portion of the earth, assuming no dependence of the variations on one horizontal (e.g. east-west) coordinate (McNish, 1938; Nagata, 1950; Forbush and Casaverde, 1961; Fambitakoye, 1973; Onwumechilli and Ogbuehi, 1967; Onwumechilli, 1967; Mersmann et al., 1979; Küppers et al., 1979; Sulzbacher et al., 1980; Carlo et al., 1982) or else in essentially three dimensions for the globe as a whole (e.g., Price and Wilkins, 1963; Rikitake, 1966; Matsushita, 1967, 1975; Stone 1971; Parkinson, 1971; Malin, 1973; Alldredge, 1976; Mishin, 1977; Malin and Gupta, 1977; Harwood and Malin, 1977; Suzuki, 1978; Yukutake and Cain, 1979; Mishin et al., 1979; Langel et al., 1980; Winch, 1981; Matsushita and Xu, 1982; Langel, 1982; Campbell, 1983). One exception has been the study of Porath et al. (1970), which attempted a field separation over a two-dimensional array of limited extent, as in the present paper. In the unrestricted class of analyses one needs some algorithm to interpolate the data between stations and, unless the entire globe is analyzed, to extrapolate beyond the outermost stations. Generally some simple form of smooth interpolation has been used, such as a cubic spline fit, a hand-drawn curve, or an early truncation of the harmonic series used to represent the data. These techniques often involve subjective judgments which can strongly affect the results, as has been demonstrated by Matsushita (in press 1983). In addition, these techniques fail to give quantitative information about how well the results represent the true field at any given point, a problem that exists even in more sophisticated techniques of analysis (e.g. Fougere, 1963; Parkinson, 1971; Bazarzhapov et al., 1976; Whaler and Gubbins, 1981).

The technique developed here belongs basically to the unrestricted class of analyses, in that a very large set of functions is fitted to the data. However, the technique also has some characteristics of model-fitting approaches, in that information about geophysical constraints on the allowed current systems is incorporated. The degree of interpolation smoothing is optimized by

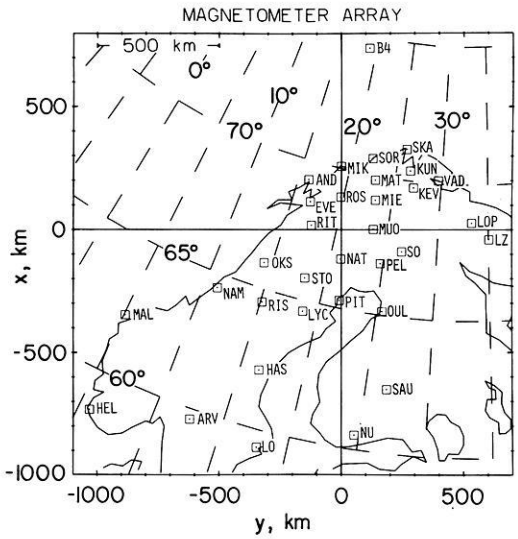

Fig. 1. Map showing locations of the magnetometers used in this study, and defining the x and y coordinates. Dashed lines give grographic latitude and longitude

adjusting it to the expected statistical characteristics of the data. A very important feature of our technique is its ability to quantify the errors involved in interpolating, separating, and mapping the magnetic variations. Without good information about these errors, which can be quite significant, it is not possible to make reliable interpretations of the estimated fields.

Data description

The data for this study come from the Scandinavian Magnetometer Array. The 33 stations used are listed in Table 1 and are shown in Fig. 1. The coordinates given in Table 1 are for the Kiruna system, defined by Küppers et al. (1979), and have the x-axis towards magnetic north (12° west of geographic north at Kiruna), the y-axis towards magnetic east, and the z-axis directed downwards. A single six-hour period is used, from 16:00 UT to 22:00 UT on 7 October 1976. For most stations three components of the magnetic variation field are available, but for a few either the vertical or horizontal components are missing, as shown in Table 1. The total number of available station-components is 94.

The data were digitized from photographic records with 10-s resolution and averaged at one-minute intervals, and a quiet-time level was subtracted out. We estimate that the combined digitization and baseline-determination errors are on the order of 5% (cf. Mersmann, 1978), a value we employ to represent random measurement error in our analysis.

This particular data set has been previously discussed by Baumjohann et al. (1978) and Küppers et al. (1979). Stacked magnetograms for one chain of stations are displayed in Fig. 2, with A, B, and Z representing variations in the x (northward), y (eastward), and z (downward) directions, respectively. From 16:00 to 18:20 UT the signature of an eastward electrojet (positive A perturbation) can be detected at all stations except B4 (Bear Island). A moderate disturbance began around 18:30 UT, when the eastward electrojet first intensified at most stations, followed by a reversal associated with the intrusion of a westward electrojet at all but the southernmost stations. At this time, the spatial pattern had important east-west as well as north-south gradients, a situation which the three-dimensional analysis technique developed in this paper is designed to handle.

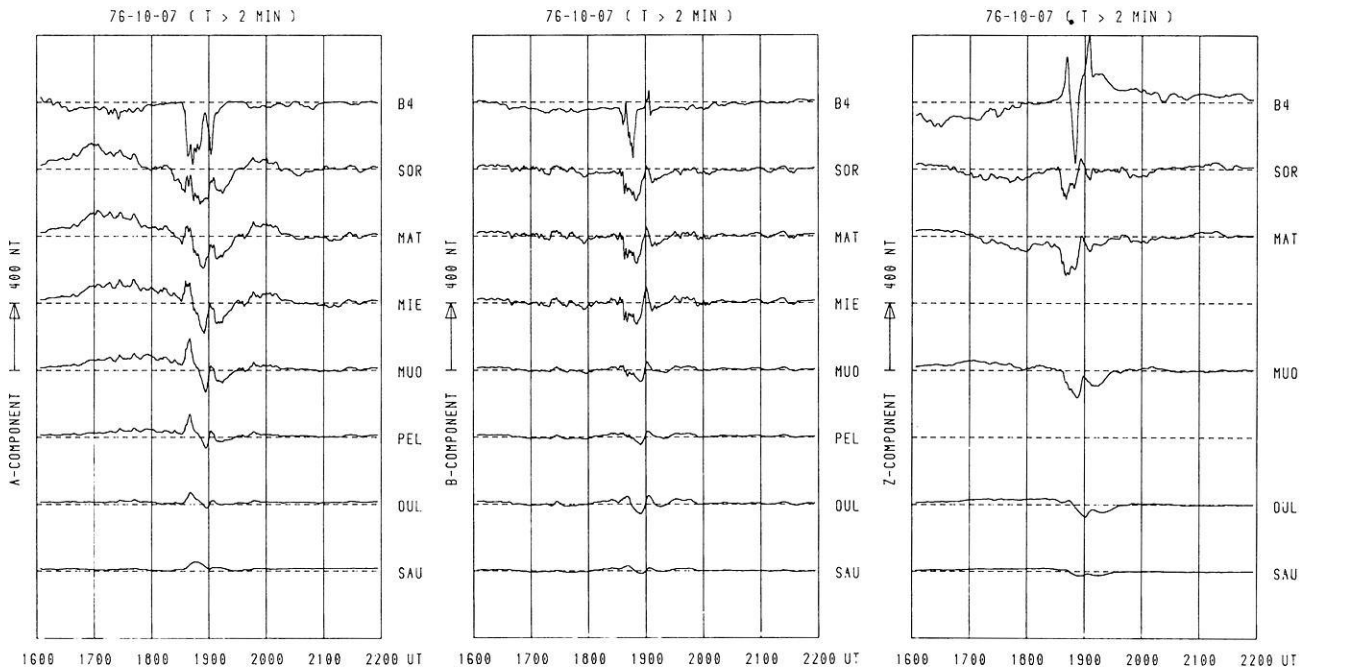

Fig. 2. Stacked magnetograms from one north-south chain of stations from 16:00 to 22:00 UT on 7 October 1976. The data have been filtered to remove periods less than about 2 min. The A, B, and Z components are in the x, y, and z directions, respectively. The distance between baselines represents 400 nT

The configuration of stations in the Scandinavian Magnetometer Array presents certain limitations on how well a spatial analysis can be performed. Except for station B4 the array essentially terminates at the Norwegian coastline, so that coverage of the strong auroral current to the north is incomplete. Furthermore, for the more rapid variations strong coastal effects associated with the internal currents just beyond the coastline affect the measurements (e.g. Küppers et al., 1979; Parkinson and Jones, 1979; Jones, 1981) but again the lack of stations beyond the coastline prevents accurate coverage of these effects. We have not attempted to quantify how these limitations might influence our data analysis procedure, but we keep them in mind in interpreting the results. We might note that the difficulty of properly handling coastal effects with land-based measurements alone arises even for the long-period S_q variations (Hobbs, 1981).

Field expansion in basis functions

We assume a plane earth model, corresponding to the Kiruna coordinate system. The magnetic variation field $b_w(x, y, z)$ (where w refers to either the x, y, or z vector component) is well represented by a magnetic potential function $V(x, y, z)$ at heights between the earth and the base of the ionosphere:

$$b_w = -\partial V/\partial w \tag{1}$$

$$\sum_w (\partial^2 V/\partial w^2) = 0 \tag{2}$$

where $\sum_w$ denotes a summation over the x, y, and z components. It is convenient to express V as a linear combination of basis functions η_j:

$$V(x, y, z) = \sum_{j=1}^{J} u_j \eta_j(x, y, z) + V'(x, y, z) \tag{3}$$

where V' is that portion of V orthogonal to the chosen finite set of basis functions. The corresponding expansion for b_w is

$$b_w = \sum_{j=1}^{J} u_j \beta_{wj} - \partial V'/\partial w \tag{4}$$

where

$$\beta_{wj} = -\partial \eta_j/\partial w. \tag{5}$$

In the present study we choose Fourier harmonics as the basis functions, so that we essentially perform the calculations in wavenumber space, and then convert back to real spatial coordinates. Fourier harmonics have the advantages of being orthogonal and having well-understood properties, but other choices could also be made, such as distributions of external and internal dipoles. The spacing of measurement points places limits on the range and resolution of harmonics that can be meaningfully determined. The maximum spacing, about 1,600 km in both the x and y directions for our data, permits a resolution of two harmonics (sine and cosine terms) per wavenumber increment of $(2\pi/1{,}600)\,\mathrm{km}^{-1}$, or one harmonic per $(\pi/1{,}600)\,\mathrm{km}^{-1}$ increment. We actually allow for a somewhat greater resolution in our analysis, with one harmonic per $(\pi/2{,}200)\,\mathrm{km}^{-1}$ increment, in order to avoid having edge effects appear too close to the outermost stations. The maximum wave-number for which useful information can be obtained is approximately π divided by the minimum measurement spacing, yielding approximately $(\pi/70)\,\mathrm{km}^{-1}$ in the x direction and $(\pi/110)\,\mathrm{km}^{-1}$ in the y direction. Because of computer limitations we actually truncate the series at somewhat smaller wavenumbers of $(\pi/107)\,\mathrm{km}^{-1}$ in x and $(\pi/122)\,\mathrm{km}^{-1}$ in y; however, it turns out that there is relatively little power in the larger wavenumbers so that not much information is lost. We choose the following basis functions over the region $x = x_0$ to $x = x_0 + \Delta x$, $y = y_0$ to $y = y_0 + \Delta y$ ($x_0 = -1{,}100$ km, $y_0 = -1{,}300$ km, $\Delta x = \Delta y = 2{,}200$ km):

$$\eta_j(x, y, z) = \sqrt{2}\cos[k_j(x - x_0)] \cdot \sqrt{2 - \delta^0_m}\cos[l_j(y - y_0)]\exp(\gamma_j z) \tag{6}$$

$$\delta^0_m = \begin{cases} 0 & \text{if } m(j) \neq 0 \\ 1 & \text{if } m(j) = 0. \end{cases} \tag{7}$$

The discrete horizontal wavenumbers k_j, l_j can be represented by

$$k_j = (n + 1/2)\pi/\Delta x, \qquad 0 \leqq n(j) \leqq N \tag{8}$$

$$l_j = m\pi/\Delta y, \qquad 0 \leqq m(j) \leqq M \tag{9}$$

where n and m are integers lying in the ranges indicated, with $N = 20$ and $M = 18$. Because (3) is a two-dimensional series n runs through its entire range for each value if m, and vice versa. (In practice, wavenumbers for which $n^2 + M^2 > N^2$ are eliminated from the series, in order to reduce the size of J.) For (2) to be satisfied, γ_j must be

$$\gamma_j = \pm\sqrt{k_j^2 + l_j^2}. \tag{10}$$

The plus sign corresponds to "internal" components of the potential, which decay with increasing altitude (negative z), while the minus sign gives "external" components of the potential, which decay with decreasing altitude. Internal-external pairs of functions exist which have identical horizontal wavenumbers but opposite signs of γ_j; for convenience of discussion we place these pairs adjacent within the series so that if j is odd η_j is an internal term and η_{j+1} is an external term. The functions η_j and η_{j+1} are themselves not orthogonal, but their gradients are, in that $\sum_w (\beta_{wj}\beta_{wj+1})$ integrated horizontally over the analysis region vanishes. The total number of basis functions used in this study is $J = 656$.

The choice of Fourier harmonics represented by (6) effectively imposes the following boundary consitions on that part of V represented by the series in (3): the north-south gradient vanishes at the northern, western, and eastern boundaries, while the east-west gradient vanishes at the southern boundary. Because b_x tends to be larger than b_y at auroral latitudes, the northern, western, and eastern boundary conditions are reasonable choices. The southern boundary condition makes less sense physically, but is mathematically convenient.

(If we had instead required each η_j to be zero on the southern boundary as well as on the northern boundary, the average value of b_x over the analysis region would be forced to vanish, a poor constraint if a dominant eastward or westward electrojet is present.) The influence of these boundary conditions on our mapping procedure is examined further below.

The representation (3) is valid only within the rectangle defined by x_0, y_0, Δx, Δy. The Fourier representation valid over all space can be written

$$V(x,y,z)=\int_{-\infty}^{\infty}dk\int_{-\infty}^{\infty}dl\{\xi^e(k,l)\cdot\exp[ik(x-x_0)+il(y-y_0)-\gamma z]+\xi^i(k,l)\exp[ik(x-x_0)+il(y-y_0)+\gamma z]\} \quad (11)$$

$$\gamma=\sqrt{k^2+l^2} \quad (12)$$

where the superscripts e and i refer to external and internal components and the number i equals $\sqrt{-1}$. The relation between the discrete coefficients u_j and the functions ξ^e, ξ^i can be obtained through multiplying the external part of (11) by η_j (j even) or the internal part by η_j (j odd) and integrating over the area of the rectangle at ground level:

$$u_j=\int_{-\infty}^{\infty}dk\int_{-\infty}^{\infty}dl\,\xi(k,l)[W_j(k,l)+W_j(-k,l)+W_j(k,-l)+W_j(-k,-l)] \quad (13)$$

$$W_j(k,l)=\frac{\sqrt{1-\delta_m^0/2}}{2}\left[\frac{\sin(k-k_j)\Delta x}{(k-k_j)\Delta x}+i\frac{1-\cos(k-k_j)\Delta x}{(k-k_j)\Delta x}\right]\times\left[\frac{\sin(l-l_j)\Delta y}{(l-l_j)\Delta y}+i\frac{1-\cos(l-l_j)\Delta y}{(l-l_j)\Delta y}\right] \quad (14)$$

where (13) applies separately for the external and internal components. The weighting functions W_j peak where $|k|=k_j$ and $|l|=l_j$ but have a finite width in $k-l$ space about these peaks, and acquire complex values away from the peaks. Thus our coefficients u_j represent some weighted average of the true spectral functions $\xi(k,l)$, so caution must be exercised in interpreting the Fourier spectrum in terms of the discrete coefficients. The problems arise mainly for small wavenumbers (long wavelengths), where the width of the weighting functions become comparable to the value of k_j or l_j. Other than pointing out this complication in the interpretation of results, we shall not pursue these effects further.

Estimation of coefficients

At any one instant of time there are I data values, consisting of one, two or three measured components of the magnetic variation vector at each station. (In the present analysis, $I=94$.) The ith data value θ_i can be expressed as

$$\theta_i=b_{w_i}(x_i,y_i,0)+\varepsilon_i=\sum_{j=1}^{J}B_{ij}u_j+v_i \quad (15)$$

$$B_{ij}=\beta_{w_i j}(x_i,y_i,0) \quad (16)$$

$$v_i=\varepsilon_i-\partial V'(x_i,y_i,0)/\partial w_i \quad (17)$$

where w_i refers to the direction of the measured component (northward, eastward, or downward), ε_i is a measurement error, assumed random. The quantity v_i represents the combination of measurement error and truncation error associated with the finite series representation of the field. The goal of our calculations is to obtain estimates $\hat{u}_j$ of the coefficients u_j by forming an appropriate linear combination of the data:

$$\hat{u}_j=\sum_{i=1}^{I}A_{ji}\theta_i. \quad (18)$$

We wish to determine coefficients A_{ji} that can be used in (18) for a large variety of data sets, taken at different times, say, comprising in effect a statistical ensemble. In order to determine the A_{ji}'s in such a way that the difference between each $\hat{u}_j$ and u_j is minimized, we apply the theory of optimal linear estimation. Specifically, if we define the estimated variation field $\hat{b}_w$ as

$$\hat{b}_w=\sum_{j=1}^{J}\hat{u}_j\beta_{wj} \quad (19)$$

then we wish to minimize the following quantity:

$$\mathrm{E}\int_{x_0}^{x_0+\Delta x}\int_{y_0}^{y_0+\Delta y}\sum_w(\hat{b}_w-b_w)^2dydx=\Delta x\Delta y\sum_{j=1}^{J}2\gamma_j^2\,\mathrm{E}[(\hat{u}_j-u_j)^2]+\mathrm{E}\int_{x_0}^{x_0+\Delta x}\int_{y_0}^{y_0+\Delta y}(\mathrm{grad}\,V')^2dydx \quad (20)$$

where E denotes the statistically expected value, or average over the ensemble.

Although we are seeking a single set of coefficients A_{ji} applicable to the entire ensemble, the coefficients will depend on the characteristics of the ensemble, and will therefore be different for ensembles with different characteristics. The ensemble can be chosen to represent a specific class of cases, such as quiet-day variations, eastward electrojets, substorms, pulsations, or variations of a particular harmonic frequency. On the other hand, the ensemble can be chosen to represent all classes of cases put together. Obviously, the more representative the ensemble is of the actual magnetic variations being analyzed at a given instant of time, the smaller the difference between $\hat{b}_w$ and b_w will be. As we shall see, we do not need detailed information about each member of an ensemble in order to find the A_{ji}'s, but rather only certain statistical measures of the ensemble as a whole. It will also be shown in the next section that the appropriate statistical measures can be estimated from the available data by application of inverse theory.

In order to determine the coefficients A_{ji} we use (18) in (20) and set derivatives with respect to each coefficient equal to zero:

$$\frac{\partial}{\partial A_{kl}}\left\{\Delta x\Delta y\sum_{j=1}^{J}2\gamma_j^2\,\mathrm{E}\left[\left(\sum_{i=1}^{I}A_{ji}\theta_i-u_j\right)^2\right]+\int_{x_0}^{x_0+\Delta x}\int_{y_0}^{y_0+\Delta y}(\mathrm{grad}\,V')^2dydx\right\}=0. \quad (21)$$

This yields

$$4\Delta x\Delta y\gamma_k^2 \mathrm{E}\left[\theta_l\left(\sum_{i=1}^{I} A_{ki}\theta_i - u_k\right)\right]=0 \tag{22}$$

and therefore

$$\sum_{i=1}^{I} A_{ki}\mathrm{E}(\theta_l\theta_i)=\mathrm{E}(\theta_l u_k) \tag{23}$$

which must hold for all indices k and l. This represents a set of equations to be solved for the A_{ki} provided the statistical properties of the variation field are known as they affect the expected value quantities in (23).

At this point it is convenient to introduce matrix notation. Let $\boldsymbol{\theta}$, $\mathbf{u}$, $\hat{\mathbf{u}}$, and $\mathbf{v}$ be column matrices of length I, J, J, and I, respectively, containing the elements θ_i, u_j, $\hat{u}_j$, and v_i. Let $\mathbf{A}$ and $\mathbf{B}$ be $J\times I$ and $I\times J$ matrices containing the elements A_{ji} and B_{ij}, respectively. Then (18) and (15) can be written

$$\hat{\mathbf{u}}=\mathbf{A}\boldsymbol{\theta} \tag{24}$$

$$\boldsymbol{\theta}=\mathbf{B}\mathbf{u}+\mathbf{v} \tag{25}$$

and the set of equations (23) can be written

$$\mathbf{A}\mathrm{E}(\boldsymbol{\theta}\boldsymbol{\theta}^T)=\mathrm{E}(\mathbf{u}\boldsymbol{\theta}^T) \tag{26}$$

where a superscript T denotes a transposed matrix. By use of (25) together with the assumption $\mathrm{E}(\mathbf{u}\mathbf{v}^T)=0$ we find

$$\begin{aligned}\mathrm{E}(\boldsymbol{\theta}\boldsymbol{\theta}^T)&=\mathrm{E}[(\mathbf{B}\mathbf{u}+\mathbf{v})(\mathbf{u}^T\mathbf{B}^T+\mathbf{v}^T)]\\&=\mathbf{B}\mathrm{E}(\mathbf{u}\mathbf{u}^T)\mathbf{B}^T+\mathrm{E}(\mathbf{v}\mathbf{v}^T)\end{aligned} \tag{27}$$

$$\mathrm{E}(\mathbf{u}\boldsymbol{\theta}^T)=\mathrm{E}[\mathbf{u}(\mathbf{u}^T\mathbf{B}^T+\mathbf{v}^T)]=\mathrm{E}(\mathbf{u}\mathbf{u}^T)\mathbf{B}^T. \tag{28}$$

Defining the moment matrices $\mathbf{C}_u$ (dimensioned $J\times J$) and $\mathbf{C}_v$ (dimensioned $I\times I$) as

$$\mathbf{C}_u=\mathrm{E}(\mathbf{u}\mathbf{u}^T) \tag{29}$$

$$\mathbf{C}_v=\mathrm{E}(\mathbf{v}\mathbf{v}^T) \tag{30}$$

we can express the solution of (26) for $\mathbf{A}$ as

$$\mathbf{A}=(\mathbf{C}_u\mathbf{B}^T)(\mathbf{B}\mathbf{C}_u\mathbf{B}^T+\mathbf{C}_v)^{-1} \tag{31}$$

where the superscript "-1" denotes an inverse matrix. This result is an expression of the Gauss-Markoff Theorem used in optimal linear estimation theory (e.g. Liebelt, 1967, Chap. 5). The key now to estimating magnetic variation patterns from the combination of (19), (24), and (31) is to know the spectral density matrix $\mathbf{C}_u$ and the error matrix $\mathbf{C}_v$. The manner in which these are determined is described in the next section.

Three additional remarks can be made concerning the optimal linear estimation technique. First, $\mathbf{C}_u$ is not the covariance matrix for $\mathbf{u}$ unless the expected value of $\mathbf{u}$ is zero, in contrast to the interpretation of Jackson (1979). Second, the matrix $\mathbf{A}$ can also be calculated as

$$\mathbf{A}=(\mathbf{C}_u^{-1}+\mathbf{B}^T\mathbf{C}_v^{-1}\mathbf{B})^{-1}\mathbf{B}^T\mathbf{C}_v^{-1} \tag{32}$$

(Liebelt, 1967; Jackson, 1979) which yields the same result as (31) but can be computationally simpler if $J<I$, that is, if more observations are available the number of basis functions. Third, the result (31) or (32) can also be obtained be requiring minimization of the following quantity for any given set of measurements:

$$\hat{\mathbf{u}}^T\mathbf{C}_u^{-1}\hat{\mathbf{u}}+(\mathbf{B}\hat{\mathbf{u}}-\boldsymbol{\theta})^T\mathbf{C}_v^{-1}(\mathbf{B}\hat{\mathbf{u}}-\boldsymbol{\theta}). \tag{33}$$

Although the physical significance of (33) is not as transparent as the meaning of (20), the minimization of quantities in the form of (33) but with a different meaning assigned to $\mathbf{C}_u$ has been the basis of mapping techniques developed elsewhere (e.g. Shure et al., 1982; Richmond and Venkateswaran, 1971; Kroehl and Richmond, 1979). We compare briefly the present technique with others in the Discussion section of this paper.

Estimation of $\mathbf{C}_u$

The moment matrix $\mathbf{C}_u$, as we shall see, contains information about the spatial power spectrum and spatial autocorrelation of the class of magnetic variations it represents, and therefore has considerably more significance than merely a mathematical quantity needed to produce optimal linear estimates of the magnetic variation patterns. Different $\mathbf{C}_u$'s can be used to represent different classes of variations (e.g., different frequency components) or, if we are content with less accuracy in our estimates, a single $\mathbf{C}_u$ can be used to represent all classes together. In principle $\mathbf{C}_u$ can be specified independently of the particular data set under analysis, provided one has independent information about the spatial power spectrum or spatial autocorrelation characteristics of the magnetic variations. Since these characteristics have not yet been determined for the Scandinavian region (nor for any other region, for that matter), we must estimate them from the available data.

For the present study we use a single $\mathbf{C}_u$ to represent the properties of the magnetic variations in the six-hour period under investigation. Ideally we would have

$$\mathbf{C}_u=\langle\mathbf{u}\mathbf{u}^T\rangle \tag{34}$$

where the angled brackets denote the time average over the period. The quantity (34) cannot be determined precisely, since we do not know what the true coefficients $\mathbf{u}$ are. Thus we have an inverse problem of trying to estimate (34) from the available observations. Bretherton and McWilliams (1980) have reviewed the application of inverse theory to the problem of fitting a power spectrum to sparse irregularly spaced data. In this paper we adopt a simpler approach than that outlined by Bretherton and McWilliams, with the justification that a fairly rough estimate of $\mathbf{C}_u$ is adequate to demonstrate our mapping technique. Our approach to estimating $\mathbf{C}_u$ has the virtues of being straightforward and of appearing to give reasonable results. It has the drawbacks of being nonrigorous and of not providing quantitative information about the accuracy of the resultant $\mathbf{C}_u$.

Our procedure is an iterative one. We begin with a first guess for $\mathbf{C}_u$ and calculate $\hat{\mathbf{u}}$ at five-minute intervals throughout the six-hour period. We then calculate the moment matrix for $\hat{\mathbf{u}}$,

$$\mathbf{C}_{\hat{u}}=\langle\hat{\mathbf{u}}\hat{\mathbf{u}}^T\rangle \tag{35}$$

$\mathbf{C}_{\hat{u}}$ is related to $\mathbf{C}_u$ by the expression

$$\mathbf{C}_{\hat{u}} = \mathbf{A}\mathbf{B}\mathbf{C}_u^T \tag{36}$$

(Liebelt, 1967, Chap. 5). It is not, however, an unbiased estimate of $\mathbf{C}_u$. In particular, the diagonal elements of $\mathbf{C}_{\hat{u}}$ tend to be smaller than the corresponding elements of $\mathbf{C}_u$. This occurs because in the presence of increasing uncertainty, the optimal estimate $\hat{\mathbf{u}}$ will tend toward zero in order to minimize the probable error. To get an unbiased estimate of $\mathbf{C}_u$, we use the following relation:

$$\mathbf{C}_u = [\mathbf{C}_u \mathbf{C}_{\hat{u}}^{-1}]\mathbf{C}_{\hat{u}} = [\mathbf{C}_u(\mathbf{A}\mathbf{B}\mathbf{C}_u^T)^{-1}]\langle \hat{\mathbf{u}}\hat{\mathbf{u}}^T \rangle. \tag{37}$$

The first guess for $\mathbf{C}_u$ is used to evaluate the right-hand side of (37), which is then used as a new estimate of $\mathbf{C}_u$. This procedure does not yield a perfectly symmetric matrix, so the result must be made symmetric by averaging the calculated $\mathbf{C}_u$ with its transposed form $\mathbf{C}_u^T$. The estimation procedure can then be further iterated.

It should be noted that the absolute magnitudes of the initially assumed $\mathbf{C}_u$ and $\mathbf{C}_v$ are irrelevant, since a multiplication of all their elements by a constant would leave $\mathbf{A}$ and the expression in square brackets in (37) unchanged. It should also be noted that this estimation procedure may not necessarily always converge, nor need it converge to the true value of $\mathbf{C}_u$. One obvious limitation, for example, is the fact that we have at most $I(I+1)/2$ independent measures of the statistical properties of the data in the symmetric matrix $\langle \boldsymbol{\theta}\boldsymbol{\theta}^T \rangle$, while $\mathbf{C}_u$ can have many more elements than this. Application of formal inverse theory techniques could help determine the accuracy of $\mathbf{C}_u$, but we do not attempt such a determination in this paper. Instead, we constrain $\mathbf{C}_u$ to be well-behaved by expressing it in terms of a relatively few number of free parameters, taking geophysical information into account in choosing the form of parameterization. The parameterization choices and the reasoning behind them are summarized below.

(1) We assume that all elements of $\mathbf{C}_u$ are zero except those elements $\langle u_i u_j \rangle$ for which $k_i = k_j$ and $l_i = l_j$, which holds only for the diagonal elements of $\mathbf{C}_u$ and for those off-diagonal elements corresponding to internal-external pairs. $\mathbf{C}_u$ is thus composed of 2×2 submatrices along its diagonal, with all other elements zero. As we shall see in the next section, this assumption essentially corresponds to spatial stationarity, for which the statistical properties of the magnetic variations are independent of horizontal location. It is a strong assumption that departs significantly from attaining the ideal representation (34), because significant off-diagonal elements can arise from spatial inhomogeneities like the increase in magnetic variation amplitudes towards the north or nonuniform earth conductivities, as well as from the fact that the average values of the coefficients do not vanish over the time interval examined. In effect, then, we should tend to produce a spectral density matrix representative of a less specialized class of variations than those of this particular data set, so that the accuracy of our subsequent field estimates is degraded. However, this assumption is extremely convenient computationally, and produces adequate results for the purposes of the present study.

(2) The external elements (j even) are parameterized as

$$\langle u_j^2 \rangle = g_1 e^{2\gamma_j H}(g_2 + \zeta_j^2/\gamma_0^2)^{-p_1} \tag{38}$$

$$\zeta_j^2 = g_3 k_j^2 + (2 - g_3) l_j^2 \tag{39}$$

where g_1, g_2, g_3, p_1 are free parameters, γ_0 is a normalizing factor, arbitrarily set to $10^{-5}\,\mathrm{m}^{-1}$, and H is 110 km, roughly the mean height of auroral ionospheric currents (e.g. Kamide and Brekke, 1977). The exponential factor in (38) accounts for geometrical attenuation between the ionosphere and the ground (remember that γ_j is negative for external terms). The manner in which k_j^2 and l_j^2 are combined to form ζ_j^2 allows for spatial anisotropy, i.e., stronger north-south than east-west magnetic variations when $0 < g_3 < 1$. Initial attempts to fit the data with a simple power law dependence of $\langle u_j^2 \rangle$ on ζ_j^2, that is, with $g_2 = 0$ in (38), produced unsatisfactory results; hence the introduction of this extra parameter.

(3) Each internal component u_j (j odd) is assumed to be partially correlated with the instantaneous external component u_{j+1} of the same horizontal scale, with the degree of correlation being a function only of γ_j as would be expected for a horizontally stratified conducting earth. That is, we assume

$$u_j = f_j u_{j+1} + u_j' \tag{40}$$

where u_j' is statistically uncorrelated with u_{j+1} and where

$$f_j = g_4(\gamma_j^2/\gamma_0^2)^{-p_2} \tag{41}$$

with g_4 and p_2 being free parameters. That a portion of u_j is uncorrelated with the instantaneous external component u_{j+1} of the same horizontal scale can be thought of as arising from two effects. First, the induced earth currents depend on the past history of the external variations and not just the instantaneous values (e.g. Nopper and Hermance, 1974; Mareschal, 1976). Second, the conductivity structure of the earth departs significantly from a horizontally stratified form (e.g. Küppers et al., 1979; Jones, 1981) so that a portion of u_j is caused by external fields of different horizontal scales than represented by u_{j+1}. For simplicity we assume that $\langle u_j'^2 \rangle$ is isotropic and of power law dependence on γ_j:

$$\langle u_j'^2 \rangle = g_5(\gamma_j^2/\gamma_0^2)^{-p_3} \tag{42}$$

where g_5 and p_3 are free parameters. With these assumption the internal diagonal elements of $\mathbf{C}_u$ become

$$\langle u_j^2 \rangle = g_5(\gamma_j^2/\gamma_0^2)^{-p_3} + f_j^2 \langle u_{j+1}^2 \rangle \tag{43}$$

and the off-diagonal elements become (with j odd)

$$\langle u_j u_{j+1} \rangle = f_j \langle u_{j+1}^2 \rangle. \tag{44}$$

In (43) and (44) the external moments $\langle u_{j+1}^2 \rangle$ (j odd) are given by (38).

In each iterative application of (37) to determine $\mathbf{C}_u$, the functional forms given above are fitted to the elements computed on the right-hand side of (37), rather than retaining the full information contained in all

Table 2. Comparison of initially assumed and finally derived parameters used to represent $\mathbf{C}_u$.

Parameter	Initial Value	Final Value
g_1	1	1.0×10^{-7} (T·m)^2
g_2	0	0.31
g_3	0.4	0.3
g_4	0.2	0.074
g_5	0.04	2.8×10^{-9} (T·m)^2
p_1	3	2.5
p_2	0	0.41
p_3	3	1.8

these elements. Consistent with this simplification, the amount of computation is greatly reduced by retaining in the matrices $\mathbf{ABC}_u^T$ and $\langle\hat{\mathbf{u}}\hat{\mathbf{u}}^T\rangle$ only those elements in the 2×2 submatrices along the diagonal, that is, only those elements corresponding to non-zero elements of the parameterized $\mathbf{C}_u$.

Since the matrix $\mathbf{A}$ involves $\mathbf{C}_v$, some knowledge of this error matrix is required in order to fit $\mathbf{C}_u$ to the data. Fortunately, for the present application we can expect $\mathbf{C}_v$ to be relatively small. We assume that the combined measurement and truncation errors are uncorrelated between the various station-components, so that $\mathbf{C}_v$ has non-zero elements only on its diagonal. Initially, we assumed that these elements were 0.0025 times the corresponding diagonal elements of $\mathbf{BC}_u\mathbf{B}^T$ in (31), representing errors v_i of approximately 5% the data values θ_i. After the second iterative application of (37) it appeared that an inadequate fit of $\mathbf{C}_u$ to the data for the higher harmonics could be ameliorated by increasing the error matrix. Supposing that the extra error might reside in small-scale (truncated) features, producing greater relative error in the vertical than horizontal components and exaggerated near the coast, we tried

$$\langle v_i^2\rangle=(\mathbf{BC}_u\mathbf{B}^T)_{ii}\times\begin{cases}0.01 & \text{for horizontal components}\\ 0.0225 & \text{for non-coastal vertical components}\\ 0.09 & \text{for coastal vertical components}\end{cases}\tag{45}$$

where the "coastal" stations are noted in Table 1. This choice improved the fit of $\mathbf{C}_u$ to the data, and for this reason alone was adopted.

Three iterations using (37) appeared to yield a resultant $\mathbf{C}_u$ very similar to what was input from the previous iteration. Details of the fitting algorithm need not be given here, but some indication of the type of agreement sought may be seen by noting the comparisons between the parameterized and computed spatial power spectra in the next section. Table 2 shows how much the final parameters differ from those initially assumed. With these specifications of $\mathbf{C}_u$ and $\mathbf{C}_v$ the root-mean-square difference between calculated and observed magnetic variations is 12% of the root-mean-square observed values for this data set.

Finally, we should point out that the fit of $\mathbf{C}_u$ to data does not of necessity require availability of a time series. The fit could also be performed with data from a single instant of time, for example, provided the number of data values is much larger than the number of parameters fit. However, the more sets of data that can be incorporated representative of the class of variations being analyzed, the more accurately can $\mathbf{C}_u$ be determined.

Properties of $\mathbf{C}_u$

The elements in the 2×2 submatrices along the diagonal of $\mathbf{C}_u$ represent the mean spatial power spectrum of magnetic variations for the period of time we are analyzing. The average value of $\langle V^2\rangle$ over the analysis region at the earth's surface can be written

$$\begin{aligned}&\frac{1}{\Delta x\Delta y}\int_{x_0}^{x_0+\Delta x}\int_{y_0}^{y_0+\Delta y}\langle V^2\rangle dx\,dy\\&=\frac{1}{4\Delta x\Delta y}\sum_{j=1}^{J}[\Phi^e(k_j,l_j)+\Phi^i(k_j,l_j)+\Phi^{ei}(k_j,l_j)]\\&\quad+\frac{1}{\Delta x\Delta y}\int_{x_0}^{x_0+\Delta x}\int_{y_0}^{y_0+\Delta y}\langle V'^2\rangle dx\,dy\end{aligned}\tag{46}$$

where

$$\Phi^e(k_j,l_j)=4\Delta x\Delta y\langle u_j^2\rangle,\qquad j\text{ even}\tag{47}$$

$$\Phi^i(k_j,l_j)=4\Delta x\Delta y\langle u_j^2\rangle,\qquad j\text{ odd}\tag{48}$$

$$\Phi^{ei}(k_j,l_j)=4\Delta x\Delta y\langle u_ju_{j+1}\rangle,\qquad j\text{ odd}.\tag{49}$$

The functions Φ^e and Φ^i are the two-dimensional power spectral densities of the external and internal components of V, and Φ^{ei} is the cross-spectral density. They have units of (magnetic potential)^2 per unit inverse wavelength in x, per unit inverse wavelength in y. The spatial power spectral densities of the vector magnetic variation components are simply related to these functions. For northward magnetic variations, the corresponding power spectral densities are just k_j^2 times Φ^e, Φ^i, and Φ^{ei}. For eastward magnetic variations, they are l_j^2 times the respective functions. For vertical magnetic variations the power spectral densities are γ_j^2 times Φ^e and Φ^i for the separate external and internal spectra, but $-\gamma_j^2$ times Φ^{ei} for the cross-spectrum.

Figure 3 shows the power spectral densities obtained from our parameterized $\mathbf{C}_u$. The solid line in Fig. 3a shows Φ^e plotted against $\gamma_j/2\pi$ for the case of $l_j=0$ (and therefore $m=0$), while the dashed line shows Φ^e plotted against $\gamma_j/2\pi$ for the case of $k_j=0$ (and therefore $n=-1/2$). The difference between these two lines results from the anisotropy of the magnetic variations with respect to the north-south and east-west directions. As an indication of how consistent these curves are with the data set we used, points are plotted which are derived with the aid of (37). These points are obtained in the following manner. First, the right-hand side of (37) is computed as discussed in the previous section. This is defined to be an estimate $\hat{\mathbf{C}}_u$ of the moment matrix $\mathbf{C}_u$. Next, the external diagonal elements of $\hat{\mathbf{C}}_u$ are normalized to correspond either to the $l_j=0$ case as

$$\hat{C}_{ujj}\times\left[\frac{g_2+\zeta_j^2/\gamma_0^2}{g_2+g_3\gamma_j^2/\gamma_0^2}\right]^{p_1}\tag{50}$$

or else to the $k_j=0$ case as

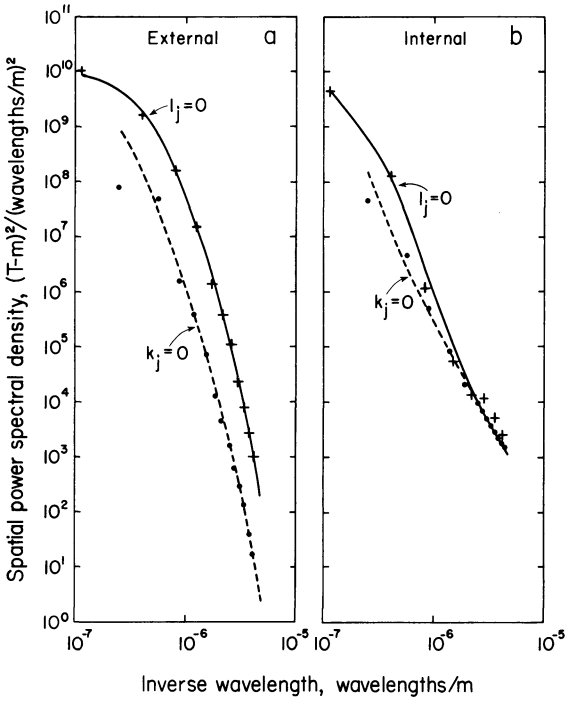

Fig. 3a and b. Spatial power spectral densities for the external **a** and internal **b** magnetic potential components from the Scandinavian Magnetometer Array data of 16:00–22:00 UT, 7 October 1976. *Solid lines* show the fitted spectral functions for variations of the north-south wavenumber, with a zero east-west wavenumber. *Dashed lines* show the spectra for variations of the east-west wavenumber, with a zero north-south wavenumber. *Crosses* and *dots*, corresponding to the solid and dashed curves, respectively, show the calculated power densities for subgroup medians of the spatial Fourier series, averaged over the six-hour time interval. See text for further explanation

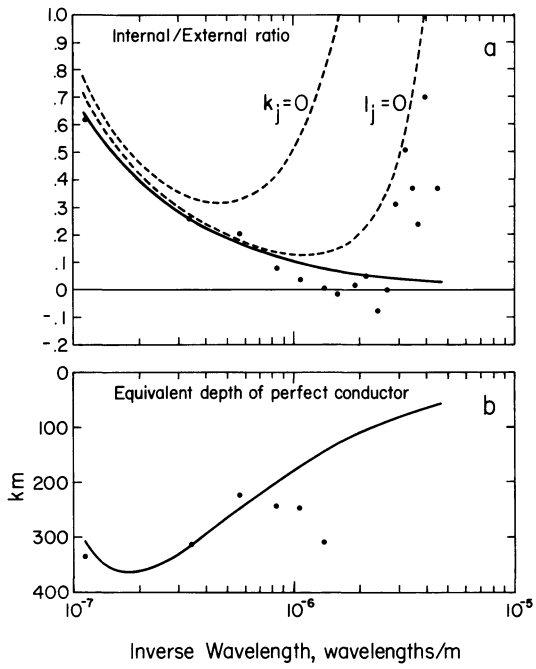

Fig. 4a and b. Derived relations between internal and external magnetic components for the Scandinavian Magnetometer Array data of 16:00–22:00 UT, 7 October 1976. **a** The *solid line* shows the function f_j, representing the ratio between the coherent fraction of the internal component and the total external component, as a function of inverse wavelength. The *points* show subset medians of this ratio obtained from the spatial Fourier series, averaged over the six-hour time interval. The *dashed lines* show the ratio of the total internal magnitude to external magnitude for horizontal wavenumbers directed north-south ($l_j=0$ curve) or east-west ($k_j=0$ curve). **b** The *curve* gives the equivalent depth of a perfectly conducting layer which could represent the function f_j according to (52). *Points* correspond to the points in **a** with small wavenumbers

$$\hat{C}_{ujj}\times\left[\frac{g_2+\zeta_j^2/\gamma_0^2}{g_2+(2-g_3)\gamma_j^2/\gamma_0^2}\right]^{p_1} \tag{51}$$

depending on which normalizing factor produces the smaller relative change. Next, for each of the two resultant sets of values, the values are grouped in subsets of 1, 3, 5, ... by increasing γ_j. Finally, for each subset, the median value is found, multiplied by $4\Delta x\Delta y$, and plotted against the median value of $\gamma_j/2\pi$ for the subset. Circles are used the $k_j=0$ case and crosses for the $l_j=0$ case. Figure 3b, for Φ^i, is obtained in an entirely analogous manner. The normalizing factors are different from the external case, but are sufficiently complex (although easily derived) that they are not written explicitly here.

Figure 4 illustrates the relations between the internal and external components. The solid line in Fig. 4a plots the function f_j, which is the ratio between the coherent fraction of the internal potential and the external potential. The points are the subset medians of $\hat{C}_{ujj+1}/\hat{C}_{uj+1j+1}$. As previously, the subsets are formed by grouping 1, 3, 5, ... values by increasing γ_j. Only a fraction of the internal magnetic variations is coherent with the same spatial scale of external variations. The total internal component is on the average larger than its coherent fraction alone. To illustrate this, we show with dashed lines the functions $(\langle u_j^2\rangle/\langle u_{j+1}^2\rangle)^{1/2}$, with j odd, for the $l_j=0$ and $k_j=0$ cases. The curves represent the ratio of the average magnitude of internal magnetic variations to the average magnitude of external variations as a function of $\gamma_j/2\pi$.

For a fixed value of γ_j the coherent portion of the internal variation can be represented by a simple model of earth conductivity involving a perfectly conducting layer at a depth D below the surface, overlain by a perfect insulator. At this conducting layer the total vertical magnetic variation must vanish, meaning that the external and internal magnetic potentials become equal. For the coherent portion of the internal potential to equal the total external potential, the depth must be

$$D=\frac{-\log f_i}{2\gamma_j}. \tag{52}$$

This depth is plotted in Fig. 4b.

The moment matrix for **u** can also be used to determine the spatial autocorrelation functions for magnetic variations. These are of interest, for instance, for the purpose of knowing how well the magnetic varia-

tion field measured at one point can be used to represent the field at some distance removed, information that is needed when correcting magnetic surveys for fluctuating fields (e.g. Regan and Rodriguez, 1981). Let us represent a particular component of the variation field at point s on the ground as

$$b_w^s = \mathbf{u}^T \boldsymbol{\beta}_w^s + r_w^s = \boldsymbol{\beta}_w^{sT} \mathbf{u} + r_w^s \tag{53}$$

where $\boldsymbol{\beta}_w^s$ is a column matrix with elements $\beta_{wj}(x_s, y_s, 0)$, and r_w^s is the truncation residual (a scalar quantity). The autocorrelation between the magnetic variations at points s and t is

$$\begin{aligned} \mathrm{E}(b_w^s b_w^t) &= \mathrm{E}[(\boldsymbol{\beta}_w^{sT}\mathbf{u} + r_w^s)(\mathbf{u}^T \boldsymbol{\beta}_w^t + r_w^t)] \\ &= \boldsymbol{\beta}_w^{sT} \mathbf{C}_u \boldsymbol{\beta}_w^t + \mathrm{E}(r_w^s r_w^t). \end{aligned} \tag{54}$$

With the simplified form we have assumed for $\mathbf{C}_u$, (54) yields the following expressions for the x, y, and z magnetic components:

$$\begin{aligned} \mathrm{E}(b_x^s b_x^t) = \sum_{\substack{j=1 \\ j\,\mathrm{odd}}}^{J} & (\langle u_j^2 \rangle + \langle u_{j+1}^2 \rangle + 2\langle u_j u_{j+1} \rangle) \\ & \cdot \beta_{xj}^s \beta_{xj}^t + \mathrm{E}(r_x^s r_x^t) \end{aligned} \tag{55}$$

$$\begin{aligned} \mathrm{E}(b_y^s b_y^t) = \sum_{\substack{j=1 \\ j\,\mathrm{odd}}}^{J} & (\langle u_j^2 \rangle + \langle u_{j+1}^2 \rangle + 2\langle u_j u_{j+1} \rangle) \\ & \cdot \beta_{yj}^s \beta_{yj}^t + \mathrm{E}(r_y^s r_y^t) \end{aligned} \tag{56}$$

$$\begin{aligned} \mathrm{E}(b_z^s b_z^t) = \sum_{\substack{j=1 \\ j\,\mathrm{odd}}}^{J} & (\langle u_j^2 \rangle + \langle u_{j+1}^2 \rangle - 2\langle u_j u_{j+1} \rangle) \\ & \cdot \beta_{zj}^s \beta_{zj}^t + \mathrm{E}(r_z^s r_z^t). \end{aligned} \tag{57}$$

Let us evaluate (57) further. We have

$$\begin{aligned} \beta_{zj}^s \beta_{zj}^t &= 2\gamma_j^2 \cos[k_j(x_s - x_0)] \cos[k_j(x_t - x_0)] \\ &\quad \cdot \sqrt{2 - \delta_m^0} \cos[l_j(y_s - y_0)] \cos[l_j(y_t - y_0)] \\ &= \gamma_j^2 \{\cos[k_j(x_s - x_t)] + \cos[k_j(x_s + x_t - 2x_0)]\} \\ &\quad \times \frac{2 - \delta_m^0}{2} \{\cos[l_j(y_s - y_t)] + \cos[l_j(y_s + y_t - 2y_0)]\}. \end{aligned} \tag{58}$$

Note that the multipliers of $\beta_{zj}^s \beta_{zj}^t$ within the summation expression in (57) are always positive. The expressions $\cos[k_j(x_s - x_t)]$ and $\cos[l_j(y_s - y_t)]$ are also positive for x_s sufficiently close to x_t and y_s sufficiently close to y_t, so that these terms make a coherent contribution to the summation, at least for small spatial separations. On the other hand, the expressions $\cos[k_j(x_s + x_t - 2x_0)]$ and $\cos[l_j(y_s + y_t - 2y_0)]$ can have any sign, in a more or less random manner, unless $l_j = 0$, or unless both points are close to the edges of our rectangle. Well within the rectangle, these terms will tend to cancel upon summation, and can be expected to contribute only a small amount to the correlation (unless $l_j = 0$). Near the edges of our rectangle the correlation is affected by our assumed boundary conditions, but because these conditions have been arbitrarily imposed, there is no justification to consider any properties of the magnetic variations in those regions. We therefore drop these latter expressions from (58)

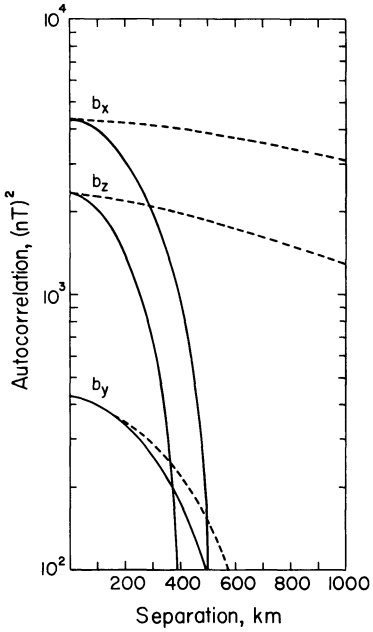

Fig. 5. Spatial autocorrelations of the total (external plus internal) magnetic variations. *Solid lines* are for separations in the north-south direction, and *dashed lines* are for separations in the east-west direction

(except when $l_j = 0$). Then we can use

$$\beta_{zj}^s \beta_{zj}^t = \gamma_j^2 \cos[k_j(x_s - x_t)] \cos[l_j(y_s - y_t)] \tag{59}$$

in (57). Quite similar reasoning allows us to use

$$\beta_{xj}^s \beta_{xj}^t = k_j^2 \cos[k_j(x_s - x_t)] \cos[l_j(y_s - y_t)] \tag{60}$$

$$\beta_{yj}^s \beta_{yj}^t = l_j^2 \cos[k_j(x_s - x_t)] \cos[l_j(y_s - y_t)] \tag{61}$$

in (55) and (56). With these replacements the autocorrelations (55) to (57) become spatially stationary, that is, dependent on the spatial separation of points s and t but independent of location. This result derives from our assumption that $\mathbf{C}_u$ has no off-diagonal terms except those coupling external and internal variations with the same horizontal wavenumber.

Figure 5 shows the autocorrelations as a function of spatial separation. The solid and dashed lines refer to separations in the north-south and east-west directions, respectively. To obtain these curves, we used the estimated $\hat{\mathbf{C}}_u$ obtained from (37) rather than the parameterized $\mathbf{C}_u$, and we assumed that

$$\mathrm{E}(r_x^s r_x^s) = 0.0075\, \mathrm{E}(b_x^s b_x^s) \tag{62}$$

$$\mathrm{E}(r_y^s r_y^s) = 0.0075\, \mathrm{E}(b_y^s b_y^s) \tag{63}$$

$$\mathrm{E}(r_z^s r_z^s) = 0.02\, \mathrm{E}(b_z^s b_z^s) \tag{64}$$

consistent with our final error matrix $\mathbf{C}_v$, with an allowance for 5% measurement error. We further assumed that $\mathrm{E}(r_w^s r_w^t)$ is essentially zero for spatial separations greater than 100 km. Between 0 and 100 km we assumed a linear decline to zero. These assumptions have little effect on the results plotted. Figure 5 shows that b_x and b_z vary relatively slowly in the east-west direction, but in the north-south direction the autocorrelations fall off rapidly, to half of their maxima at

distances of 280 km for b_x and 230 km for b_z. Beyond these separations a measurement made at one point would be a poor representation of the magnetic variation at another point. The autocorrelation of the b_y component decreases by similar rates in both the north-south and east-west directions, to half its maximum at distances of 350 km and 410 km, respectively. Unlike the b_x and b_z components, the b_y component receives no contribution from east-west aligned auroral currents, which give b_x and b_z their extended autocorrelations in the east-west direction.

Estimation of mapping errors

Related to the problem of determining spatial autocorrelation functions for the magnetic variation field components is the problem of determining the expected error of the estimated magnetic variations as they are mapped out over the rectangle. Unlike the autocorrelation function, however, the mapping error depends on the location of the point under consideration in relation to the configuration of observing points. The expected mapping error depends on the statistical properties of the field as contained in $\mathbf{C}_u$ and $\mathbf{C}_v$, as well as on the locations of available data, and can be discussed without reference to any specific data values. We therefore introduce the relative mapping errors in this section before proceeding to show mapping results for the magnetic variations in the next section.

The relative error of any estimated quantity depends not only on location, but also on the type of quantity under consideration. For example, estimated magnetic field variations generally have a larger relative error than does the magnetic potential at the same point, because the magnetic field has a stronger weighting of the higher harmonics in the Fourier series than does the potential, and these higher harmonics are found to have larger relative errors than the lower harmonics. Similarly, the magnetic potential continued upward to the ionosphere has larger relative errors than the field at ground level, in part because of the faster exponential growth of the higher harmonics than of the lower harmonics during upward continuation. In this section we present maps of relative error for two types of quantities: for the external vector field and the internal vector field, both at ground level. It should be borne in mind that these computed errors are strictly valid only for the specific quantities concerned, and do not apply quantitatively to other quantities such as to the magnetic potential, or even to the b_x, b_y, or b_z component alone. Nevertheless, the mapping of these computed errors is of great value in obtaining an overall picture of how valid are our estimated variation fields presented in the next section.

The mean square error for one magnetic field component at a given point is:

$$\begin{aligned}\mathrm{E}[(\hat{b}_w - b_w)^2] &= \mathrm{E}\{[\boldsymbol{\beta}_w^T(\hat{\mathbf{u}}-\mathbf{u})+r_w][(\hat{\mathbf{u}}-\mathbf{u})^T\boldsymbol{\beta}_w + r_w]\} \\ &= \boldsymbol{\beta}_w^T\mathbf{C}_{\hat{u}-u}\boldsymbol{\beta}_w + \mathrm{E}(r_w^2) \end{aligned} \tag{65}$$

where we have dropped the superscripts denoting location because only one location is under consideration at a time. The error moment matrix is

$$\mathbf{C}_{\hat{u}-u} \equiv \mathrm{E}[(\hat{\mathbf{u}}-\mathbf{u})(\hat{\mathbf{u}}-\mathbf{u})^T] = \mathbf{C}_u - \mathbf{C}_{\hat{u}} = \mathbf{C}_u - \mathbf{A}\mathbf{B}\mathbf{C}_u^T \tag{66}$$

(Liebelt, 1967). Expression (65) gives the mean square error for the total (external plus internal) field components. We can obtain the error for the external portion alone by zeroing out all elements of $\boldsymbol{\beta}_w$ corresponding to the internal portion (j odd). Similarly, the error for the internal part can be obtained by zeroing out all elements of $\boldsymbol{\beta}_w$ with even j. The mean square error of the vector field is the sum of the mean square errors of the x, y, and z components. Dividing this by the mean square value of the field yields the square of the relative error. Defining Δ^e as the relative error for the external component and Δ^i as the relative error for the internal component we have

$$\Delta^{e\,2} = \frac{\sum_w (\boldsymbol{\beta}_w^{eT}\mathbf{C}_{\hat{u}-u}\boldsymbol{\beta}_w^e) + \rho^{e\,2}}{\sum_w \mathrm{E}(b_w^{e\,2})} \tag{67}$$

$$\rho^{e\,2} \equiv \sum_w \mathrm{E}(r_w^{e\,2}) \tag{68}$$

$$\Delta^{i\,2} = \frac{\sum_w (\boldsymbol{\beta}_w^{iT}\mathbf{C}_{\hat{u}-u}\boldsymbol{\beta}_w^i) + \rho^{i\,2}}{\sum_w \mathrm{E}(b_w^{i\,2})} \tag{69}$$

$$\rho^{i\,2} \equiv \sum_w \mathrm{E}(r_w^{i\,2}) \tag{70}$$

where the superscripts e and i now denote external or internal, rather than referring to station location. Because wavelengths shorter than our cutoff are expected to be strongly attenuated from the ionosphere to the ground, we can neglect ρ^e, and set it to zero. If the truncation error is nearly all internal, then it should be on the order of one-third the total internal variation, to be consistent with our final specification of $\mathbf{C}_v$. We therefore set $\rho^{i\,2}$ equal to 0.11 times the denominator of (69).

Figure 6 shows the relative errors obtained by evaluating the square roots of expressions (67) and (69) at 50 km intervals over the area of interest. The area plotted is identical to that of Fig. 1, but is somewhat smaller than the rectangle defined by the boundaries of our calculations, because near these boundaries the arbitrarily imposed boundary conditions have a strong influence on the results. The minimum relative error in the external component is 9%, occurring in the area where measurements are most dense. The mapping error increases rapidly beyond the outermost stations. The relative error in the internal component is everywhere large, with a minimum of 42% where measurements are most dense. It is clearly difficult to extract the complex internal variation in the presence of a considerably larger external variation. The error noted here refers to a single instant of time, however, so that statistical processing of the internal component for a long time series can produce more significant results. In order to compare the absolute errors between the external and internal components, the relative errors should be multiplied by the root-mean-square external and internal variations (the square roots of the denominators in (67) and (69)), which are 85 nT and 30 nT, respectively. The external absolute error is generally somewhat smaller than the internal error in the region

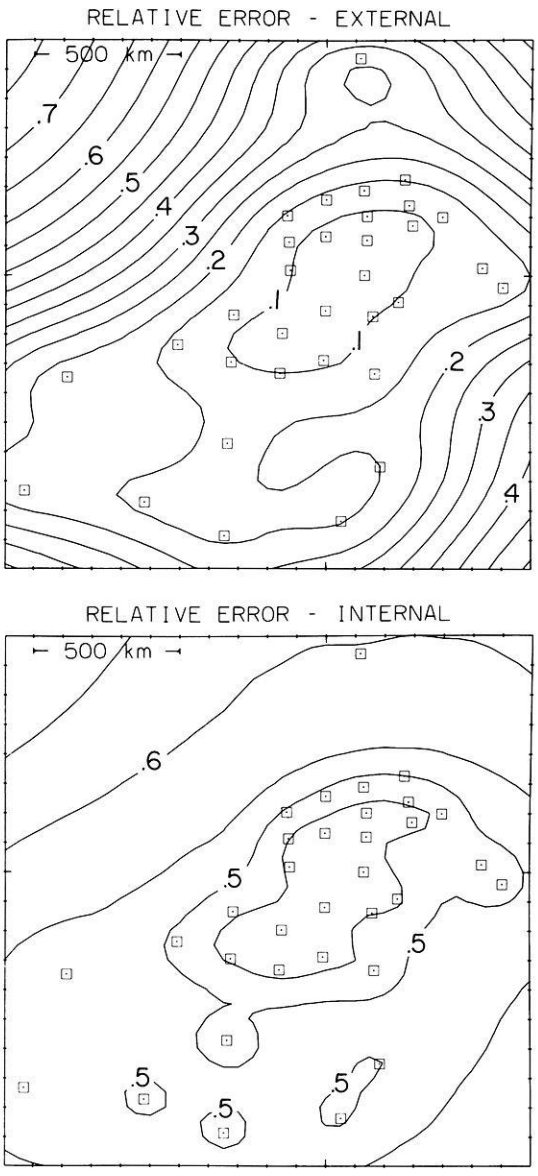

Fig. 6. Fractional expected error in the derived magnetic variation field for the external and internal components at ground level as a function of location. The contour interval is 0.05

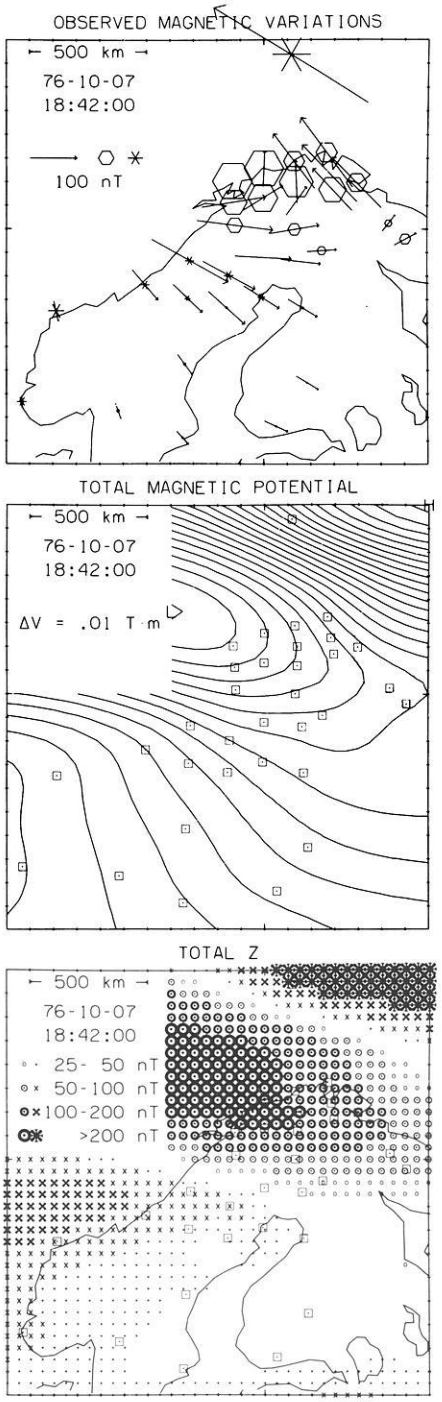

Fig. 7. Maps of ground-level magnetic variation patterns at 18:42 UT on 7 October 1976. *Top:* Horizontal magnetic variations are shown by vectors rotated 90° clockwise to represent "equivalent" currents. Vertical variations are shown by *hexagons* (upward) or *stars* (downward). *Middle:* The total (external plus internal) magnetic potential $\hat{V}$ is contoured at intervals of 0.01 T·m. "H" and "L" show the high and low potential values in the plotting region. *Bottom:* The total (external plus internal) vertical magnetic variation component $\hat{b}_z$ is represented at 50-km intervals by *circular* (upward) or *cross* (downward) symbols

of highest station density, but becomes larger than the internal error away from this region. Because of simplified assumptions we made in estimating $\mathbf{C}_u$, these mapping errors should be considered lower limits.

Sample mapping results

Figure 7 shows a sample of input data and resultant estimated fields $\hat{V}$ and $\hat{b}_z$ (labelled "total Z") mapped over the same area as in Figs. 1 and 6, that is, somewhat inside the boundaries of the rectangle defined by x_0, $x_0+\Delta x$, y_0 and $y_0+\Delta y$. The horizontal magnetic vectors have been rotated clockwise by 90° to make visual comparison with contours of $\hat{V}$ easier. These vectors have been called "equivalent current vectors", as they represent the direction and strength of a horizontal current sheet directly overhead which could produce them. The time chosen, 18:42 UT, represents a penetration of strong westward equivalent current (the westward electrojet) in the northern part of the displayed region, together with an intensification of the eastward equivalent current (eastward electrojet) in the center.

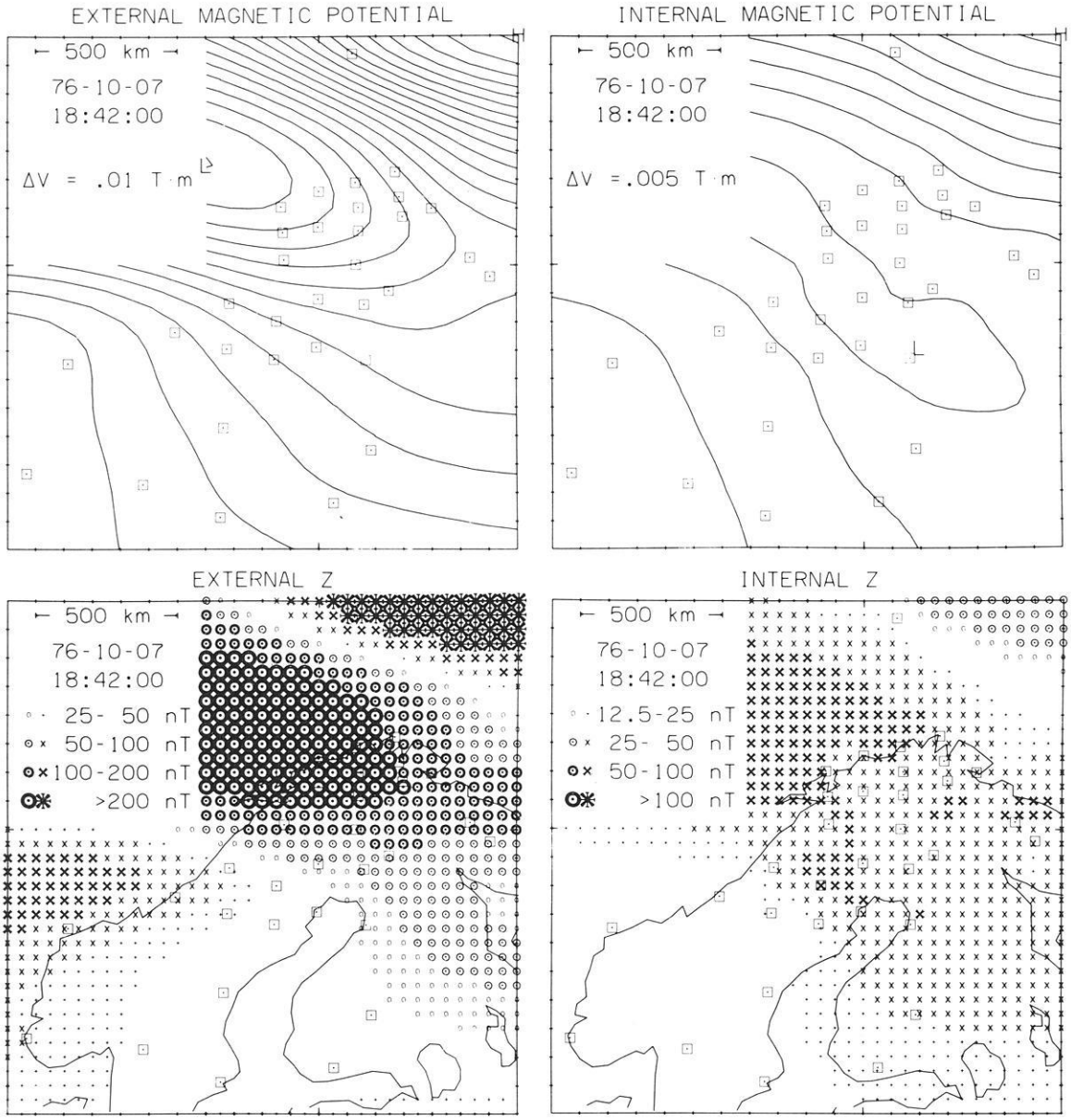

Fig. 8. Maps of external and internal magnetic variation patterns at 18:42 UT on 7 Obtober 1976. *Upper left:* The external component of the magnetic potential $\hat{V}^e$ is contoured at intervals of 0.01 T·m. *Upper right:* The internal magnetic potential V^i is contoured at intervals of 0.005 T·m. *Lower left:* The external component of the vertical magnetic variation field $\hat{b}_z^e$ is represented at 50-km intervals by *circular* (upward) or *cross* (downward) symbols. *Lower right:* The internal vertical magnetic variation is represented with twice the sensitivity of the external component

This configuration of equivalent currents is a manifestation of the so-called "Harang discontinuity" (Harang, 1946; Heppner, 1972) which normally occurs in the late evening hours at auroral latitudes.

Figure 8 shows the separation of the magnetic potential and vertical field into external and internal components. The internal field is considerably weaker than the external, and is therefore plotted with greater sensitivity. A tendency for the external and internal magnetic potentials to correlate positively is discernable, as is a tendency for the b_z components to correlate negatively, but these tendencies are rather weak in detail. Notice that there is an enhancement of the internal b_z at the location of the Storavann anomaly discussed by Jones (1981).

Figure 9 shows the external part of $\hat{V}$ at a height of 110 km, roughly in the region where strong ionospheric currents are known to flow. Small-scale features are noticeably amplified in the process of upward continuation of the field, and the error associated with the field estimation also grows substantially. If the electric currents responsible for the field flowed entirely in a thin shell just above 110 km, the magnetic potential contours would correspond to isolines of current flow, with 15.9 kA of "equivalent current" flowing between contours spaced at 0.01 T·m intervals. The amplification of errors in going up to 110 km means that features like the weakening of the westward equivalent just north of the Norwegian coast should not be considered realistic. There simply exists inadequate infor-

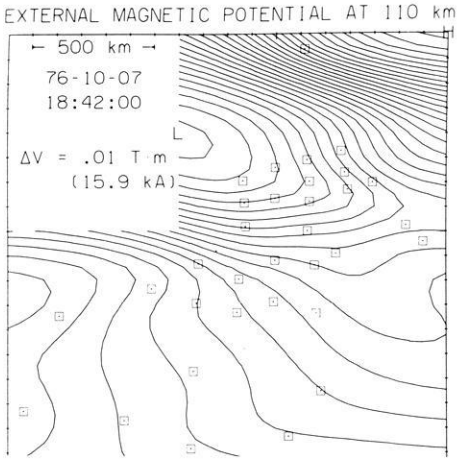

Fig. 9. The external component of the magnetic potential at 110-km altitude is contoured at intervals of 0.01 T·m, representing the magnetic effects of an equivalent sheet current with 15.9 kA flowing between contours counterclockwise about the potential low (L)

mation to be able to determine the true magnetic potential pattern in such regions. Further south, where the station density is adequate to determine some finer-scale structure of the field at ionospheric heights, the sharp kinks of the contours near $x=-200$ km may be realistic, corresponding to the southern edge of aurorally enhanced conductivities. South of this line, the magnetic field variations are probably associated largely with remote non-ionospheric currents, particularly those flowing to great heights along geomagnetic field lines.

Effect of changed boundary conditions

As pointed out above we cannot adequately resolve wavenumbers between $0\,\mathrm{km}^{-1}$ and about $(\pi/1{,}600)$ km^{-1} due to the limited array extent, even though a large part of the power lies in these small wavenumbers. For this small-wavenumber component of the spectrum the boundary conditions implied in the choice of basis functions can have an appreciable effect on the calculated distribution of variations with respect to wavenumber. In order to test the importance of this we calculated the fields for reversed northern and southern boundary conditions, that is, with basis functions satisfying

$$\eta_j = 0 \qquad \text{at } x = -1{,}100\,\mathrm{km} \tag{71}$$

$$\partial\eta_j/\partial x = 0 \qquad \text{at } x = 1{,}100\,\mathrm{km}. \tag{72}$$

This was achieved simply be replacing $\cos[k_j(x-x_0)]$ by $\sin[k_j(x-x_0)]$ in (6). The moment matrix $\mathbf{C}_u$ was kept the same as before.

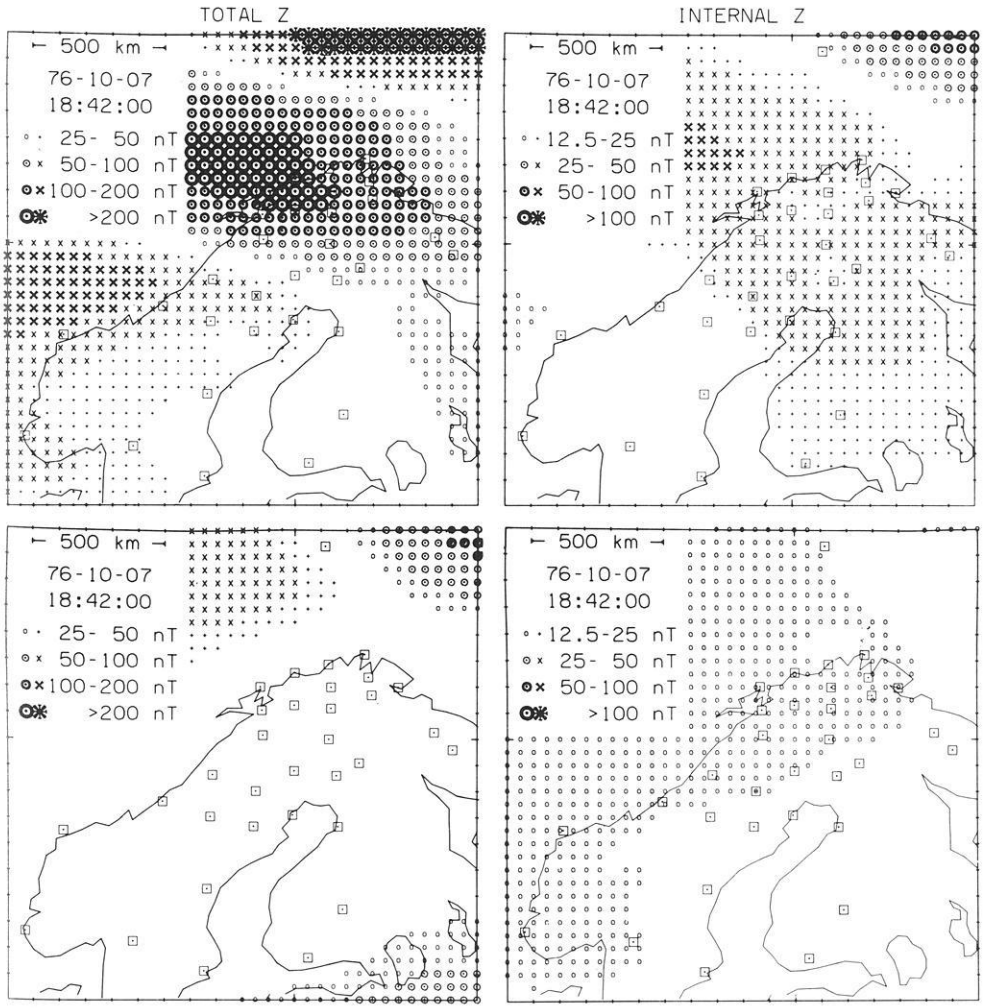

Fig. 10. Maps of vertical variation fields at 18:42 UT on 7 October 1976, showing effects of changed boundary conditions. *Upper left:* The total (external plus internal) component $\hat{b}_z$ is represented at 50-km intervals by *circular* (upward) or *cross* (downward) symbols. *Upper right:* The internal component is represented with twice the sensitivity of the total field. *Lower left:* The difference between the field above and that in Fig. 7 shows changes in data-poor regions. *Lower right:* The difference between the field above and that in Fig. 8 shows boundary-condition effects on large-scale features

Figure 10 shows, at the top, the resultant total b_z and internal component of b_z mapped over the data region (which is smaller than the analysis region defined by the boundaries of the calculations). Again the internal component is plotted with doubled sensitivity. The bottom half of Fig. 10 shows the differences between the fields above and the corresponding fields in Figs. 7 and 8. Not surprisingly, the total b_z field is in close agreement between the two calculations in the vicinity of the measurement points, and diverges only some distance away these points. Significant differences do appear in separating the external and internal fields, however, differences that affect the internal component relatively more than the external component. It is seen in the difference field that the effect is primarily a large-scale feature, which would be associated with the long-wavelength components of the field. These results illustrate the facts noted previously by Gough (1973), Banks (1973), Frazer (1974), Lilley (1975), Singh (1980), and Gough and Ingham (1983), that an analysis over a limited area cannot accurately represent the true spectrum of long-wavelength features or permit an accurate separation of long-wavelength internal and external components. It is important to note, however, that the total long-wavelength field is well represented over the measurement region, even of it cannot be accurately broken down by wavenumber or accurately separated into internal and external components.

Comparison between two- and three-dimensional separations

It is of interest to see how much difference in the field separation there exists between the three-dimensional technique of this study and a simpler two-dimensional technique using only the northward and vertical variation measurements from a single chain of stations, assuming no east-west gradient of the variations. Mersmann (1978) and Lange (1979) have analyzed in some detail how accurately a two-dimensional separation can be performed for the Scandinavian data. In particular, they have shown that the results of the separation are influenced by the type of assumptions made in extrapolating the observations beyond the last stations in the profile. Since our present interest is to determine differences caused only by incorporating or ignoring east-west gradients, we need to use comparable interpolation and extrapolation procedures in performing the three- and two-dimensional separations. We therefore set up the two-dimensional separation making only the following changes from our three-dimensional algorithm:

(1) Only terms with $m=0$ were kept in the Fourier series.

(2) Only one chain of stations was used (Stations B4, SOR, MAT, MIE, MUO, PEL, OUL, and SAU).

(3) Only the A and Z data values were used.

We chose a time, 18:42 UT, for which there is considerable east-west structure, in order to make a fairly severe test of the two-dimensional separation procedure.

Figure 11 compares the computed ground-level $\hat{b}_x$ and $\hat{b}_z$ external and internal profiles for the two separation procedures. The curves are plotted over the entire range of calculation, from x_0 to $x_0+\Delta x$, in order to show the nature of the assumed boundary conditions. In obtaining the curves from the three-dimensional calculation the y coordinate is linearly interpolated between the stations and linearly extrapolated beyond SAU and B4. Small oscillations at the truncation wavelength are noticeable but not dominant. The differences between the two- and three-dimensional separations are perhaps smaller than one might have expected. The percentage differences in the external components are relatively small, but in the internal components the percentage differences are more significant, particularly in $\hat{b}_z^i$ over the Scandinavian mainland. In general, the differences appear to be no greater than the inherent mapping error in the three-dimensional technique, which is shown in Fig. 6. A test for a different time when the auroral electrojet had a more nearly two-dimensional structure, at 17:30 UT, yielded even better agreement between the two- and three-dimensional techniques. Thus in many circumstances the two-dimensional approximation for field separation may give satisfactory results, even when significant east-west structure is present. Nevertheless, greater accuracy may be expected from the three-dimensional technique, and this added accuracy may be helpful in some studies, particularly those of internal variations.

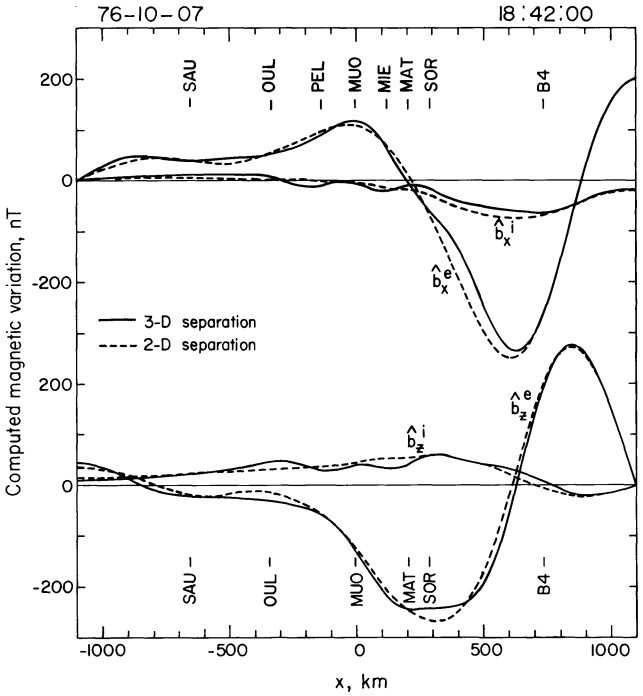

Fig. 11. Comparison between magnetic field separation results from the three-dimensional and two-dimensional formulations (see text) at 18:42 UT on 7 October 1976. Solid lines show the 3-D separation results, and dashed lines shown the 2-D separation results. $\hat{b}_x^e$ and $\hat{b}_x^i$ are the external and internal northward components, while $\hat{b}_z^e$ and $\hat{b}_z^i$ are the external and internal downward components. The locations of the stations used are shown by short vertical lines labelled by the station abbreviation. No vertical data were available from the stations PEL and MIE

Discussion

The theoretical framework developed in this paper makes possible more accurate analyses of magnetic variation spatial patterns than have been possible with previously employed techniques. By incorporating knowledge of the expected statistical characteristics of the variations and measurements, as contained in the moment matrices $\mathbf{C}_u$ and $\mathbf{C}_v$, we essentially acquire some advantages of model-fitting approaches while retaining the generality and flexibility of unrestricted analysis techniques. For the usual case where a priori information about $\mathbf{C}_u$ and $\mathbf{C}_v$ may be deficient, we have shown that estimates of these matrices can be constructed with the aid of the available data. Knowledge of these matrices, or of the spatial correlation functions of the magnetic variations, allows us to quantify the expected errors incurred when the field is mapped over the region of interest. Quantification of errors, although very important for making reliable interpretations of mapped variation fields, has not previously been attempted to the extent presented in this paper.

A comparison between the technique we use in this paper with a sample of techniques developed elsewhere helps to clarify the advantages and disadvantages of different approaches to mapping fields from point measurements. We note first of all that our attempt to incorporate statistical information in order to constrain the behaviour of the field differs fundamentally from techniques that make no a priori assumptions about the field characteristics for any given set of measurements. Oldenburg (1976b), for example, applied the linear inverse theory of Backus and Gilbert (1970) to the problem of estimating a Fourier spectrum from a limited set of point measurements. He made essentially no a priori assumptions about the spectral form (apart from his suggestion of improving results by interpolating through data gaps - a procedure that implies some information about the spectral content). His work helps to clarify the possible wavenumber resolution attainable and the tradeoff between resolution and accuracy. Ordinary least-squares fits to data effectively minimize a quantity like

$$(\mathbf{B}\hat{\mathbf{u}}-\boldsymbol{\theta})^T\mathbf{C}_v^{-1}(\mathbf{B}\hat{\mathbf{u}}-\boldsymbol{\theta}) \tag{73}$$

and therefore also assume nothing about the spectral content of the data; i.e., since $\mathbf{C}_u^{-1}$ is set to zero in (33), the ensemble needed to construct $\mathrm{E}(\mathbf{u}\mathbf{u}^T)$ is unbounded. In ordinary least-squares fits the matrix $\mathbf{C}_v$ is often considered to consist only of measurement errors, with no account taken of truncation errors, even though the latter are often important because of the need to truncate J at some level less than I. If the measurements are not well-spaced, ordinary least-squares fits often tend to yield unrealistic results in regions of sparse data.

Shure et al. (1982) developed a mapping technique designed for application to the whole-earth main geomagnetic field, motivated in part by the problem of estimating the field in past epochs from relatively sparse data. Their procedure is similar to minimization of (33), except that they actually minimize a quantity like

$$\hat{\mathbf{u}}^T\mathbf{F}\hat{\mathbf{u}} \tag{74}$$

where $\mathbf{F}$ is some prespecified positive definite $J\times J$ matrix, with the constraint that

$$(\mathbf{B}\hat{\mathbf{u}}-\boldsymbol{\theta})^T\mathbf{C}_v^{-1}(\mathbf{B}\hat{\mathbf{u}}-\boldsymbol{\theta})=S^2 \tag{75}$$

where S^2 is some prespecified constant. They showed how $\mathbf{F}$ can be specified by minimizing some physical quantity like the magnetic energy outside the earth's core, in which case $\mathbf{F}$ becomes diagonal, and illustrated how different mapping results are obtained with different choices for $\mathbf{F}$ and S^2 (including $S^2=0$). Our study, along with work by McLeod (1983), suggests that their technique would yield optimal results if $\mathbf{F}$ is chosen to correspond to the spatial power spectrum as it appears in $\mathbf{C}_u^{-1}$; good empirical estimates of this power spectrum are now available for the main field (e.g., Langel and Estes, 1982; Ostrowski, 1982; McLeod, 1983). There also exists an optimal choice of S^2, obtainable by combining (24) and (75). The algorithms developed by Richmond and Venkateswaran (1971) and by Kroehl and Richmond (1979) for mapping magnetic variation fields are similar to that of Shure et al. (1982), effectively minimizing a quantitiy of the form

$$\hat{\mathbf{u}}^T\mathbf{F}\hat{\mathbf{u}}+(\mathbf{B}\hat{\mathbf{u}}-\boldsymbol{\theta})^T\mathbf{C}_v^{-1}(\mathbf{B}\hat{\mathbf{u}}-\boldsymbol{\theta}). \tag{76}$$

This is similar to (33), except that $\mathbf{F}$ was determined by a combination of arguments about the expected smoothness properties of the variation field plus trial-and-error attempts to obtain desirable results. Non-diagonal weighting matrices $\mathbf{F}$ were involved. These algorithms can obviously also stand improvement in order to yield more nearly optimal results.

In principal, our technique provides optimal results under the condition (24) that the coefficients are a linear combination of the observations. Jackson (1979) and Tarantola and Valette (1982) have discussed how further improvements in the estimation of coeffcients from data can be achieved when a valid a priori estimate is available, corresponding in our case to an estimate of the expected value of $\mathbf{u}$. In this case one deals with the covariance matrix for $\mathbf{u}$ (i.e., the moment matrix $\mathrm{E}([\mathbf{u}-\mathrm{E}(\mathbf{u})][\mathbf{u}-\mathrm{E}(\mathbf{u})]^T)$ rather than the moment matrix $\mathbf{C}_u$; the methods become identical when $\mathrm{E}(\mathbf{u})=0$. Tarantola and Valette (1982) applied their technique to an example of curve-fitting, that is, interpolation and extrapolation, and also discussed optimal estimation techniques for the case where the data and desired parameters are not linearly related.

As pointed above our assumption of spatial stationarity greatly simplifies the numerical analysis, but does not realistically account for localized anomalies like the coast effect. One way to modify the technique to account for nonstationarity would be to allow more off-diagonal terms in $\mathbf{C}_u$. Another possible approach would be to use basis functions of a localized character, either in place of or in conjunction with Fourier harmonics, in order to minimize the number of affected elements in $\mathbf{C}_u$. We would also expect significant improvement in the mapping if $\mathbf{C}_u$ is subdivided into several matrices, each representing a restricted class of magnetic variations. Subdivision by temporal frequency would be especially valuable, not only because the induction of earth currents is frequency dependent, but

also because the external component of magnetic variations appears to have different spatial scales for different temporal frequencies (e.g. Kamide et al., 1969). These shortcomings of our simple $\mathbf{C}_u$ notwithstanding, the resultant mapped fields appear to be generally reasonable. In any event, it is clear that the assumed spectral form of $\mathbf{C}_u$ does not impose a fixed spatial spectrum upon the mapped field; otherwise our iteration procedure for estimating $\mathbf{C}_u$ would not have yielded a different result than what was initially assumed.

The availability of spatially mapped magnetic variation fields and quantitive knowledge of their errors facilitates a number of further geophysical studies. The external field, continued upward to the ionosphere, can be combined with information on ionospheric conductivities to yield not only the horizontal ionospheric current distribution, but also the distribution of magnetic-field-aligned currents between the ionosphere and outer magnetosphere (study in progress). For earth conductivity studies the fields can be filtered by wavenumber as well as by frequency to permit a more accurate and versatile application of induction theory. The total long-wavelength field in the region of measurement, composed of the combined external and internal components with wavelengths longer than the maximum station separation, should well meet the requirements of studies that assume the field to be large-scale, such as geomagnetic deep sounding analyses which make use of horizontal spatial gradients in the long-wavelength limit (e.g. Berdichevskiy et al., 1969a, b, 1976; Kuckes, 1973; Lilley, 1975; Lilley and Sloane, 1976; Woods and Lilley, 1979; Jones 1980; Camfield, 1981; Beamish and Johnson, 1982). A more rigorous separation of variation fields into "normal" and "anomalous" components may also be facilitated, especially since the "anomalous" component of interest should be contained entirely in the internal field which the mapping technique can in principle extract. For this purpose, however, an allowance for non-stationarity may be desirable. Overall, the availability of mapped fields and error estimates provides us with new avenues for exploring geomagnetic variations.

Acknowledgments. We are grateful to A.G. Jones for useful discussions concerning currents induced in the earth and the nature of local anomalies in the internal variation field. We also wish to thank all other coauthors and all institutions and persons acknowledged in the paper by Küppers et al. (1979) for their help in obtaining the Scandinavian Magnetometer Array data. This work received partial financial support from the Deutsche Forschungsgemeinschaft (W.B.) and from NASA Order Number W-15,347 (ADR).

References

Akasofu, S.-I., Kisabeth, J., Romick, G.J., Kroehl, H.W., Ahn, B.-H.: Day-to-day and average magnetic variations along the IMS Alaska meridian chain of observatories and modeling of a three-dimensional current system. J. Geophys. Res. **85**, 2065–2078, 1980

Alldredge, L.R.: Effects of solar activity on annual means of geomagnetic components. J. Geophys. Res. **81**, 2990–2996, 1976

Backus, G., Gilbert, F.: Uniqueness in the inversion of inaccurate gross earth data. Phil. Trans. R. Soc. A **266**, 123–192, 1970

Banks, R.J.: Data processing and interpretation in geomagnetic deep sounding. Phys. Earth Planet. Inter. **7**, 339–348, 1973

Bannister, J.R., Gough, D.I.: Development of a polar magnetic substorm: a two-dimensional magnetometer array study. Geophys. J.R. Astron. Soc. **51**, 75–90, 1977

Bannister, J.R., Gough, D.I.: A study of two polar magnetic substorms with a two-dimensional magnetometer array. Geophys. J.R. Astron. Soc. **53**, 1–26, 1978

Baumjohann, W., Greenwald, R.A., Küppers, F.: Joint magnetometer array and radar backscatter observations of auroral currents in northern Scandinavia. J. Geophys. **44**, 373–383, 1978

Baumjohann, W., Pellinen, R.J., Opgenoorth, H.J., Nielsen, E.: Joint two-dimensional observations of ground magnetic and ionospheric electric fields associated with auroral zone currents: current systems associated with the local break-ups. Planet. Space Sci. **29**, 431–447, 1981

Bazarzhapov, A.D., Mishin, V.M., Shpynev, G.B.: A mathematical analysis of geomagnetic variation fields. Gerlands Beitr. Geophys. **85**, 76–82, 1976

Beamish, D.: Source field effects on transfer functions at mid-latitudes. Geophys. J.R. Astron. Soc. **58**, 117–134, 1979

Beamish, D., Johnson, P.M.: Difficulties in the application of magnetic field gradient analysis to induction analysis. Phys. Earth Planet. Inter. **28**, 1–13, 1982

Berdichevskiy, M.N., Van'yan, L.L., Faynberg, E.B.: Magnetovariation sounding by using spatial derivatives of the field. Geomagn. Aeron. **9**, 299–301 (Engl. trans.), 1969a

Berdichevskiy, M.N., Van'yan, L.L., Faynberg, E.B.: Theoretical principles in using electromagnetic variations to study the electrical conductivity of the earth. Geomagn. Aeron. **9**, 465–467 (Engl. trans.), 1969b

Berdichevsky, M.N., Fainberg, E.B., Rotanova, N.M., Smirnov, J.B., Vanjan, L.L.: Deep electromagnetic investigations. Ann. Géophys. **32**, 143–155, 1976

Bretherton, F.P., McWilliams, J.C.: Estimations from irregular arrays. Rev. Geophys. Space Phys. **18**, 789–812, 1980

Camfield, P.A.: Magnetometer array study in a tectonically active region of Quebec, Canada. Geophys. J.R. Astron. Soc. **65**, 553–570, 1981

Campbell, W.H.: A description of the external and internal quiet daily variation currents at North American locations for a quiet-sun year. Geophys. J.R. Astron. Soc. **73**, 51–64, 1983

Carlo, L., Singh, B.P., Rastogi, R.G., Agarwal, A.K.: The induced effects of geomagnetic variations in the equatorial region. J. Geophys. **51**, 199–205, 1982

Czechowsky, P.: Calculation of an equivalent current system in the polar E-region. Radio Sci. **6**, 247–253, 1971

Fambitakoye, O.: Effects induits par l'électrojet équatorial au centre de l'Afrique. Ann Géophys. **29**, 149–169, 1973

Fambitakoye, O., Mayaud, P.N.: Equatorial electrojet and regular daily variations S_R, I. A determination of the equatorial electrojet parameters. J. Atmos. Terr. Phys. **38**, 1–17, 1976

Forbush, S.E., Casaverde, M.: Equatorial electrojet in Peru. Carnegie Inst. Washington Publ. 620, Washington, 1961

Fougere, P.F.: Spherical harmonic analysis, I. A new method and its verification. J. Geophys. Res. **68**, 1131–1139, 1963

Frazer, M.C.: Geomagnetic deep sounding with arrays of magnetometers. Rev. Geophys. Space Phys. **12**, 401–420, 1974

Gough, D.I.: The interpretation of magnetometer array studies. Geophys. J.R. Astron. Soc. **35**, 83–98, 1973

Gough, D.I., Bannister, J.R.: A polar magnetic substorm observed in the evening sector with a two-dimensional magnetometer array. Geophys. J.R. Astron. Soc. **55**, 435–450, 1978

Gough, D.I., Ingham, M.R.: Interpretation methods for magnetometer arrays. Rev. Geophys. Space Phys. **21**, 805–827, 1983

Harang, L.: The mean field of disturbance of polar geomagnetic storms. Terr. Magn. Atmos. Electr. **51**, 353–380, 1946

Harwood, J.M., Malin, S.R.C.: Sunspot cycle influence on the geomagnetic field. Geophys. J.R. Astron. Soc. **50**, 605–619, 1977

Heppner, J.P.: The Harang discontinuity in auroral belt ionospheric currents. Geofys. Publ. **29**, 105–120, 1972

Hermance, J.F., Peltier, W.R.: Magnetotelluric fields of a line current. J. Geophys. Res. **75**, 3351–3356, 1970

Hibbs, R.D., Jones, F.W.: Electromagnetic induction in three-dimensional structures for various source fields. J. Geomagn. Geoelectr. **30**, 1–18, 1978

Hobbs, B.A.: A comparison of Sq analyses with model calculations. Geophys. J.R. Astron. Soc. **66**, 435–444, 1981

Horning, B.L., McPherron, R.L., Jackson, D.D.: Application of linear inverse theory to a line current model of substorm current systems. J. Geophys. Res. **79**, 5205–5210, 1974

Hughes, T.J., Oldenburg, D.W., Rostoker, G.: Interpretation of auroral oval equivalent current flow near dusk using inversion techniques. J. Geophys. Res. **84**, 450–456, 1979

Hutton, R.: Some problems of electromagnetic induction in the equatorial electrojet region, I. Magneto-telluric relations. Geophys. J.R. Astron. Soc. **28**, 267–284, 1972

Jackson, D.D.: The use of a priori data to resolve non-uniqueness in linear inversion. Geophys. J.R. Astron. Soc. **57**, 137–157, 1979

Jones, A.G.: Geomagnetic induction studies in Scandinavia, I. Determination of the inductive response function from the magnetometer array data. J. Geophys. **48**, 181–194, 1980

Jones, A.G.: Geomagnetic induction studies in Scandinavia, II. Geomagnetic depth sounding, induction vectors and coast effects. J. Geophys. **50**, 23–36, 1981

Kamide, Y., Brekke, A.: Altitude of the eastward and westward auroral electrojets. J. Geophys. Res. **82**, 2851–2853, 1977

Kamide, Y., Iijima, T., Fukushima, N.: Microstructure of auroral-zone electrojet. Rep. Ionos. Space Res. Jpn. **23**, 185–208, 1969

Kroehl, H.W., Richmond, A.D.: Magnetic substorm characteristics described by magnetic potential maps for 26–28 March 1976. In: Dynamics of the magnetosphere, S.-I. Akasofu, ed.: pp 269–286. Dordrecht: D. Reidel, 1979

Kuckes, A.F.: Relations between electrical conductivity of a mantle and fluctuating magnetic fields. Geophys. J.R. Astron. Soc. **32**, 119–131, 1973

Küppers, F., Untiedt, J., Baumjohann, W., Lange, K., Jones, A.G.: A two-dimensional magnetometer array for ground-based observations of auroral zone electric currents during the International Magnetospheric Study (IMS). J. Geophys. **46**, 429–450, 1979

Lange, K.: Induktionseffekte in Nordskandinavien – untersucht am Beispiel zweier ostwärts fließender polarer Elektrojets. Diplomarbeit, Inst. f. Geophys. Univ. Münster, FRG, 1979

Langel, R.A.: Results from the Magsat mission. Johns Hopkins APL Tech. Digest **3**, 307–324, 1982

Langel, R.A., Estes, R.H.: A geomagnetic field spectrum. Geophys. Res. Lett. **9**, 250–253, 1982

Langel, R.A., Estes, R.H., Mead, G.D., Fabiano, E.B., Lancaster, E.R.: Initial geomagnetic field model from Magsat vector data. Geophys. Res. Lett. **7**, 793–796, 1980

Liebelt, P.B.: An introduction to optimal estimation. Reading, Mass.: Addison-Wesley Publ. Co. 1967

Lilley, F.E.M.: Magnetometer array studies: A review of the interpretation of observed fields. Phys. Earth Planet. Inter. **10**, 231–240, 1975

Lilley, F.E.M., Sloane, M.N.: On estimating electrical conductivity using gradient data from magnetometer arrays. J. Geomagn. Geoelectr. **28**, 321–328, 1976

Loginov, G.A., Vasil'ev, E.P., Grafe, A.: Some results of the investigation of magnetic variations of the auroral electrojets concluded from observations of the geomagnetic meridian project (GMP). Gerlands Beitr. Geophys. **87**, 249–262, 1978

Malin, S.R.C.: Worldwide distribution of geomagnetic tides. Phil. Trans. R. Soc. A **274**, 551–594, 1973

Malin, S.R.C., Gupta, J.C.: The Sq current system during the International Geophysical Year. Geophys. J.R. Astron. Soc. **49**, 515–529, 1977

Mareschal, M.: On the problem of simulating the earth's induction effects in modeling polar magnetic substorms. Rev. Geophys. Space Phys. **14**, 403–409, 1976

Matsushita, S.: Solar quiet and lunar daily variation fields. In: Physics of geomagnetic phenomena, S. Matsushita and W.H. Campbell, eds.: pp 301–427. New York: Academic Press, 1967

Matsushita, S.: Morphology of slowly-varying geomagnetic external fields – a review. Phys. Earth Planet. Inter. **10**, 299–312, 1975

Matsushita, S.: Cautions with spherical harmonic data analyses for the estimation of equivalent current systems. Planet. Space Sci., in press 1983

Matsushita, S., Xu, W.-Y.: Sq and L currents in the ionosphere. Ann. Geophys. **38**, 295–305, 1982

Maurer, H., Theile, B.: Parameters of the auroral electrojet from magnetic variations along a meridian. J. Geophys. **44**, 415–426, 1978

McLeod, M.G.: Optimal processing of satellite-derived magnetic anomaly data. Phys. Earth Planet. Inter. **31**, 10–26, 1983

McNish, A.G.: Heights of electric currents near the auroral zone. Terr. Magn. Atmos. Electr. **43**, 67–75, 1938

Mersmann, U.: Zweidimensionale Auswertung und Interpretation des Magnetfeldes eines ostwärts fließenden polaren Electrojets über Skandinavien. Diplomarbeit, Inst. f. Geophys. Univ. Münster, FRG, 1978

Mersmann, U., Baumjohann, W., Küppers, F., Lange, K.: Analysis of an eastward electrojet by means of upward continuation of ground-based magnetometer data. J. Geophys. **45**, 281–298, 1979

Mishin, V.M.: High-latitude geomagnetic variations and substorms. Space Sci. Rev. **20**, 621–675, 1977

Mishin, V.M., Bazarzhapov, A.D., Shpynev, G.B.: Electric fields and currents in the earth's magnetosphere. In: Dynamics of the magnetosphere, S.-I. Akasofu, ed.: pp 249–268. Dordrecht: D. Reidel, 1979

Nagata, T.: On the auroral zone current. Rep. Ionos. Res. Jpn. **4**, 87–101, 1950

Nopper, R.W., Jr., Hermance, J.F.: Phase relations between polar magnetic substorm fields at the surface of a finitely conducting earth. J. Geophys. Res. **79**, 4799–4801, 1974

Oldenburg, D.W.: Ionospheric current structure as determined from ground-based magnetometer data. Geophys. J.R. Astron. Soc. **46**, 41–66, 1976a

Oldenburg, D.W.: Calculation of Fourier transforms by the Backus-Gilbert method. Geophys. J.R. Astron. Soc. **44**, 413–431, 1976b

Onwumechilli, A.: Geomagnetic variations in the equatorial zone. In: Physics of geomagnetic phenomena, S. Matsushita and W.H. Campbell, eds.: pp 425–507. New York: Academic Press 1967

Onwumechilli, A., Ogbuehi, P.O.: Analysis of the magnetic field of the equatorial electrojet. J. Atmos. Terr. Phys. **29**, 553–566, 1967

Ostrowski, J.A.: Spectra of the International Geomagnetic Reference Field and its secular variation. J. Geomagn. Geoelectr. **34**, 417–422, 1982

Parkinson, W.D.: An analysis of the geomagnetic diurnal variation during the Int. Geophys. Year 6. Gerlands Beitr. Geophys. **80**, 199–232, 1971

Parkinson, W.D., Jones, F.W.: The geomagnetic coast effect. Rev. Geophys. Space Phys. **17**, 1999–2015, 1979

Porath, H.D., Oldenburg, D.W., Gough, D.I.: Separation of magnetic variation fields and conductive structures in the western United States. Geophys. J.R. Astron. Soc. **19**, 237–260, 1970

Price, A.T.: The theory of magnetotelluric fields when the source field is considered. J. Geophys. Res. **67**, 1907–1918, 1962

Price, A.T.: Electromagnetic induction within the earth. In: Physics of geomagnetic phenomena, S. Matsushita and W.H. Campbell, eds.: pp 235–298. New York: Academic Press 1967

Price, A.T., Wilkins, G.A.: New methods for the analysis of geomagnetic fields and their application to the Sq field of 1932–33. Phil. Trans. R. Soc. A **256**, 31–98, 1963

Quon, C., Vozoff, K., Hoversten, M., Morrison, H.F., Lee, K.-H.: Localized source effects on magnetotelluric apparent resistivities. J. Geophys. **46**, 291–299, 1979

Regan, R.D., Rodriguez, P.: An overview of the external magnetic field with regard to magnetic surveys. Geophys. Surveys **4**, 255–296, 1981

Richmond, A.D., Venkateswaran, S.V.: Geomagnetic crochets and associated ionospheric current systems. Radio Sci. **6**, 139–164, 1971

Rikitake, T.: Electromagnetism and the earth's interior. Amsterdam: Elsevier Publ. Co. 1966

Rokityansky, I.I.: Geoelectromagnetic investigation of the earth's crust and mantle. Berlin: Springer-Verlag 1982

Schmucker, U.: Regional induction studies: a review of methods and results. Phys. Earth Planet. Inter. **7**, 365–378, 1973

Shure, L., Parker, R.L., Backus, G.: Harmonic splines for geomagnetic modelling. Phys. Earth Planet. Inter. **28**, 215–229, 1982

Singh, B.P.: Geomagnetic sounding of conductivity anomalies in the lower crust and uppermost mantle. Geophys. Surv. **4**, 71–87, 1980

Srivastava, S.P.: Method of interpretation of magnetotelluric data when source field is considered. J. Geophys Res. **70**, 945–954, 1965

Stone, D.J.: The calculation of current systems of daily geomagnetic variations. Gerlands Beitr. Geophys. **80**, 117–128, 1971

Sulzbacher, H., Baumjohann, W., Potemra, T.A.: Coordinated magnetic observations of morning sector auroral zone currents with Triad and the Scandinavian Magnetometer Array: a case study. J. Geophys. **48**, 7–17, 1980

Suzuki, A.: Geomagnetic Sq field at successive universal times. J. Atmos. Terr. Phys **40**, 449–463, 1978

Tarantola, A., Valette, B.: Generalized nonlinear inverse problems solved using the least square criterion. Rev. Geophys. Space Phys. **20**, 219–232, 1982

Wait, J.R.: Theory of magnetotelluric fields. J. Res. NBS **66** D, 509–539, 1962

Walker, J.K.: Space-time associations of the aurora and magnetic disturbance. J. Atmos. Terr. Phys. **26**, 951–958, 1964

Whaler, K.A., Gubbins, D.: Spherical harmonic analysis of the geomagnetic field: an example of a linear inverse problem. Geophys. J.R. Astron. Soc. **65**, 645–693, 1981

Winch, D.E.: Spherical harmonic analysis of geomagnetic tides, 1964–1965. Phil. Trans. R. Soc. A **303**, 1–104, 1981

Woods, D.V., Lilley, F.E.M.: Geomagnetic induction in central Australia. J. Geomagn. Geoelectr. **31**, 449–458, 1979

Yukutake, T., Cain, J.C.: Solar cycle variations of the first-degree spherical harmonic components of the geomagnetic field. J. Geomagn. Geoelectr. **31**, 509–544, 1979

Received September 15, 1982; Revised July 9, 1983
Accepted September 22, 1983